

Fundamental Limits on Parametric Shape Estimation Performance

Robinson Piramuthu, Alfred O. Hero

Abstract

This paper considers the problem of extraction of shape information from noise corrupted images acquired from a resolution limited imaging instrument, a problem that is closely related to shape estimation and segmentation. The problem is formulated as estimation of coefficients in a basis expansion of the boundary of 2D and 3D star-shaped objects. We derive an expression for the Fisher information matrix and the Cramèr–Rao (CR) bound under a polar shape descriptor model, homogeneous object intensity, Gaussian point spread function, and additive white Gaussian noise. We analyze boundary estimation performance for both finite and infinite dimensional sets of shape basis functions. We show that circles and spheres are the easiest to estimate in the sense that they minimize the CR bound over the class of star shaped 2D and 3D objects, respectively. We show that irregularly shaped objects with sharp corners are worst case shapes in the sense that they maximize the CR bound. Finally we discuss the CR bound sensitivity with respect to variation of the center point position for the star-shaped object. In particular, the object centroid is not in general the optimum center location.

Index Terms: Parametric shape estimation, star-shaped objects, Cramèr–Rao bound, Fisher information, B-splines, estimator performance limits.

¹A. Hero (corresponding author) is with the Dept. of Electrical Engineering and Computer Science, the Dept. of Biomedical Engineering and the Dept. of Statistics at The University of Michigan, Ann Arbor, MI 48109-2122. R. Piramuthu was with the Dept. of Electrical Engineering and Computer Science at the University of Michigan, Ann Arbor, and is now with KLA-TENCOR, Milpitas, CA 95035. This work was supported in part by National Institutes of Health grant RO1-CA-54362.

I. INTRODUCTION

In this paper we derive the Fisher information and the Cramèr-Rao (CR) bound for 2D and 3D shape estimation problems which are applicable to the class of smooth star-shaped objects. The CR bound is an important and useful quantity since it permits comparisons between unbiased estimators of shape parameters and an estimator-independent lower bound. The CR bound and its associated Fisher information can also be used to explore the intrinsic sensitivity of shape estimator variance to object shape variations, imaging system imperfections, and noise. This allows the study of classes of shapes that are inherently simple or inherently difficult to estimate with low variance for a given class of shape models. Furthermore, as shown in [11], the shape-estimator Fisher information plays an important role in minimax fusion of shape imagery and associated functional imagery of the same imaging volume, e.g. as arises in fusion of anatomical MRI scans to functional PET scans in medical imaging. This is very important in applications such as diagnosis of medical images where shape extraction gives vital information about organ or tumor anatomy. Depending on prior knowledge about the a priori class of shapes of the organ or tumor, one can assess statistical reliability of the extracted information.

Shape extraction and segmentation methods can be either non-parametric or model-based. Grey level *thresholding* is the simplest and most wide-spread non-parametric shape extraction technique [29]. While computationally cheap and fast, thresholding methods are very sensitive to noise. Another of the difficulties with thresholding methods is the choice of threshold. Usually, the threshold is determined from the histogram [26] or by optimizing certain criterion such as connectivity of edges. If the object has a varying intensity level, using a single global threshold [19] may not perform well. In such cases, the image can be partitioned and local thresholds determined for subimages. Other non-parametric methods for shape extraction use *edge detection operators* such as Laplacian [1], Sobel [28], Kirsch [18], Marr-Hildreth [22] and Canny [4] operators. This is usually followed by other processing such as thresholding, median filtering, boundary tracing or *Hough transformation* [12], [14].

As contrasted to non-parametric shape estimation, parametric approaches to shape extraction are model-based. Examples of parametric methods include: *Fourier descriptors* [31], [36], piecewise polynomials such as *Bezier curves*, *B-splines* or *Beta-splines* [3], [37], and spherical harmonic expansions [23], [5]. These parametric methods require the object to be star-shaped, i.e. its boundary is uniquely specified by some radial function in polar (2D shapes) or spherical (3D shapes) coordinates with origin located at a center of description inside the object. It is for such models that the CR bounding approach in this paper are applicable. Star shaped models have been applied to a very wide ranging set of applications areas including: three dimensional brain segmentation [17], estimating shape torsion and scale relative to a reference shape [10], viral imaging and structure determination [39]. The results of this paper permit

exploration of fundamental estimation theoretic limitations for these and other applications.

There also exist model-based shape extraction schemes which do not require star-shaped object models, e.g., *snakes* [16], [20], [21], [24], [25], [27], [38] and *deformable templates* [2], [6], [15]. However, the specification of CR bounds for these models requires a different approach than that described in this paper.

The focus of this paper is on *parametric* shape extraction for star-shaped objects whose boundary function is representable as a linear combination of *a priori* known set of basis functions. The covariance of any estimator can be used to quantify uncertainty in any unbiased estimate. It is well-known that the covariance of any estimator can be bounded from below by the inverse of the Fisher information (the CR bound) as long as the estimator is unbiased. We obtain expressions for the Fisher information and its inverse for 2D and 3D shape estimation under the assumptions of homogeneous Gaussian additive noise, constant object intensity, and system resolution characterized by a Gaussian blur function. Simple asymptotic expressions for Fisher information are obtained which are applicable to the case of fine spatial resolution of the imaging. The Fisher information depends on factors such as contrast between the interior and background intensities, noise and blur levels in the observed image, shape of the object to be estimated, and on *a priori* constraints (for example, smoothness imposed by a selected finite basis). More significantly, for 2D shapes the Fisher information depends on the (angular) speed of the curve describing the shape boundary. The particular speed function arising here is a measure of deviation from circularity of the shape boundary. For 3D shapes the Fisher information depends on a speed function which is a generalization to surfaces of the concept of speed of a curve. Finally, we explore the extremal shapes which maximize and minimize the CR bound. For 2D shapes of fixed perimeter we establish that disk-shaped objects are the easiest to estimate while flower-shaped objects are the hardest to estimate among the class of objects representable by the B-spline basis. Similar results are shown for 3D shapes. The sensitivity of the CR bound to the center of description is also investigated.

An outline of the paper is as follows. First, we specify the model assumptions in Section 2. In Section 3, we give expressions for Fisher information and the CR bound for 2D shapes supported on a finite basis set. Under some additional assumptions we also treat the case of an infinite (complete) basis in this section. Then we study extremal shapes for both the finite and infinite dimensional basis sets. In Section 4, we study the effect of changing the center-of-description (all the while retaining a star-shaped curve) on the CR bound. An extension of the theory to 3D shapes is presented in Section 5. Most of the proofs are relegated to appendices in order to improve the flow of the paper.

II. 2D SHAPE MODEL

In this section, we define the model for uncorrupted image, observed image and feature of shape/region of interest.

A. Model for Uncorrupted Image

An object of uniform intensity on a uniform background in 2D or 3D euclidean space is specified by its shape or boundary, which is either a closed curve in 2D or a closed surface in 3D. Let θ denote a parameterization that completely describes the shape and let R_θ denote the interior of the object. Define the indicator function \mathbf{I}_{R_θ} for the region R_θ as follows:

$$\mathbf{I}_{R_\theta}(\mathbf{x}) = \begin{cases} 1, & \text{if } \mathbf{x} \in R_\theta \\ 0, & \text{o.w.} \end{cases} \quad (1)$$

Thus, the exterior (complement) of R_θ can be indicated by $1 - \mathbf{I}_{R_\theta}(\mathbf{x})$.

Let the object have a uniform intensity $C_{\text{INT}} > 0$ over R_θ and let the background intensity over the complement of R_θ be $C_{\text{BG}} > 0$. The uncorrupted image can then be represented as

$$\mathbf{I}_\theta(\mathbf{x}) = C_{\text{INT}} \cdot \mathbf{I}_{R_\theta}(\mathbf{x}) + C_{\text{BG}} \cdot (1 - \mathbf{I}_{R_\theta}(\mathbf{x})). \quad (2)$$

The contrast of the object within the image is $|C_{\text{INT}} - C_{\text{BG}}|$.

B. Model for Observed Data

Let the observed data $Y_M(\mathbf{x})$ be

$$Y_M(\mathbf{x}) = (\mathbf{I}_\theta ** H)(\mathbf{x}) + n(\mathbf{x}), \quad (3)$$

where $**$ denotes convolution, $H(\cdot)$ is the system spatial response and $n(\cdot)$ is system noise. We assume the point spread function $H(\cdot)$ to be a spatial invariant symmetric Gaussian with blur parameter σ_s , and the additive noise $n(\cdot)$ to be zero mean white Gaussian with power spectral density σ_n^2 . This restriction to Gaussian point spread is not a severe limitation for many imaging modalities and it simplifies the analysis to follow.

C. Model for Boundary

We assume that the object interior R_θ is a star-shaped region and can therefore be described by a radius function $r(\phi)$ as a scalar function of angle $\phi \in [-\pi, \pi)$, with respect to some origin O specified inside R_θ . We refer to O as the *center-of-description*. We additionally assume that the shape can be described by a linear combination of basis functions $\{B_i(\phi)\}_{i=1}^K$ in the sense that

$$r_\theta(\phi) = \mathbf{B}^T(\phi) \theta, \quad (4)$$

where $\mathbf{B}(\phi) = [B_1(\phi), \dots, B_K(\phi)]^T$ is a vector of linearly independent basis functions on $[-\pi, \pi)$. Some basis sets used to represent closed boundaries are periodic planar curve models such as Fourier descriptors, fitting of line

segments, cubics, Bezier curves, Beta-splines and B-splines [3]. When the B_i 's are taken from a complete basis set $\{B_i\}_{i=1}^{\infty}$, any L_2 bounded curve r_{θ} has the representation $r_{\theta}(\Phi) = \sum_{i=1}^{\infty} \theta_i B_i(\phi)$, $\phi \in [-\pi, \pi)$.

III. 2D SHAPE ESTIMATION

Here we consider the CR bound for two cases of 2D shape estimation, namely, *finite* and *infinite* dimensional collections of basis functions.

A. Cramèr–Rao Bound for Finite Dimensional Case

For this case the number K of basis elements is finite. The finite dimensional CR bound is a lower bound on the $K \times K$ estimator covariance matrix associated with any unbiased estimator $\hat{\theta}$ of θ

$$\text{cov}_{\theta}(\hat{\theta}) \geq \mathbf{F}_{\theta}^{-1}, \quad (5)$$

where \mathbf{F}_{θ} is the Fisher information matrix [7], [13]. The inequality in the CR bound is shorthand notation for: $\text{cov}_{\theta}(\hat{\theta}) - \mathbf{F}_{\theta}^{-1}$ is a non-negative definite matrix.

The Fisher information matrix \mathbf{F}_{θ} was derived in [33] for the model (3) and (4):

$$\mathbf{F}_{\theta} = C_{\text{CN}} \iint_{-\pi}^{\pi} \exp \left[-\frac{\|\vec{r}_{\theta}(\phi) - \vec{r}_{\theta}(\gamma)\|^2}{4\sigma_s^2} \right] r_{\theta}(\phi) r_{\theta}(\gamma) \mathbf{B}(\phi) \mathbf{B}^T(\gamma) d\phi d\gamma \quad (6)$$

where

$$C_{\text{CN}} = \frac{(C_{\text{INT}} - C_{\text{BG}})^2}{4\pi\sigma_n^2\sigma_s^2} = \frac{(\text{contrast})^2}{4\pi\sigma_n^2\sigma_s^2}$$

is the normalized contrast and $\vec{r}_{\theta}(\phi)$ represents the radius vector of the boundary at angle ϕ . Thus, $\|\vec{r}_{\theta}(\phi) - \vec{r}_{\theta}(\gamma)\|$ is the Euclidean distance between boundary points $\vec{r}_{\theta}(\phi)$ and $\vec{r}_{\theta}(\gamma)$. More details on this expression can be found in [33, pp. 58–60] and [11]. The CR bound for covariance of $\hat{r}(\cdot)$, an unbiased estimate of $r_{\theta}(\cdot)$ that also lies in the span of the given basis set, is given by $\text{CRB}_{r,\theta}(\phi, \gamma) = \mathbf{B}^T(\phi) \mathbf{F}_{\theta}^{-1} \mathbf{B}(\gamma)$ and an asymptotic form was shown in [11] as

$$\text{CRB}_{r,\theta}(\phi, \gamma) = \frac{1}{2\sqrt{\pi}\sigma_s C_{\text{CN}}} \mathbf{B}^T(\phi) \left[\int_{-\pi}^{\pi} h_{\theta}(\psi) \mathbf{B}(\psi) \mathbf{B}^T(\psi) d\psi \right]^{-1} \mathbf{B}(\gamma) + o(\sigma_m) \quad (7)$$

where

$$h_{\theta}(\psi) := \frac{r_{\theta}^2(\psi)}{\sqrt{r_{\theta}^2(\psi) + [r'_{\theta}(\psi)]^2}} \quad (8)$$

$$\sigma_m := \max_{\phi} \left\{ \frac{\sqrt{2}\sigma_s}{\|\vec{r}'_{\theta}(\phi)\|} \right\} = \max_{\phi} \left\{ \frac{\sqrt{2}\sigma_s}{\sqrt{[r_{\theta}(\phi)]^2 + [r'_{\theta}(\phi)]^2}} \right\} \quad (9)$$

and $r'_{\theta}(\phi) := dr_{\theta}(\phi)/d\phi$.

The quantity $\sqrt{[r_{\theta}(\phi)]^2 + [r'_{\theta}(\phi)]^2}$ gives the magnitude of rate at which the radius vector changes with angle and is known as the (angular) “speed” [30] of the curve. Hence we refer to σ_m in (9) as the maximum resolution–speed ratio. Note that σ_m decreases when the shape is magnified. On the other hand, when σ_m is small, the spatial resolution is high enough to resolve finer details in the boundary shape.

B. Interpretation of $h_{\theta}(\psi)$

The quantity $h_{\theta}(\psi)$ from (8) has some interesting interpretations not discussed in [11]. Refer to Figure 1. It can be shown that the distance from the center–of–description O to the tangent line at P is

$$\frac{r_{\theta}^2(\psi)}{\sqrt{r_{\theta}^2(\psi) + \left(\frac{dr_{\theta}(\psi)}{d\psi}\right)^2}}$$

. To see this consider the segment OA in Figure 1: $OA = OP \sin(\pi - \tau) = OP \sin \tau$. Therefore, $OA = \frac{r_{\theta}(\psi) \tan \tau}{\sqrt{1 + \tan^2 \tau}}$. It is easily shown that $\tan \tau = \frac{r_{\theta}(\psi)}{\partial r_{\theta}(\psi)/\partial \psi}$ [32, pp. 473]. Thus, $OA = h_{\theta}(\psi)$.

We therefore conclude that $h_{\theta}(\psi)$ is the distance between the center–of–description and the tangent line to the boundary at angle ψ . For fixed perimeter this distance is obviously minimized for a circular boundary. Also note that $h_{\theta}(\psi)$ can be written as a ratio of $r_{\theta}(\psi)$ (same dimensions as perimeter) and the dimensionless quantity $\sqrt{1 + \left[\frac{r'_{\theta}(\psi)}{r_{\theta}(\psi)}\right]^2}$. This dimensionless quantity is the ratio of speed [30] of the curve at angle ψ to the speed of a circle of radius $r_{\theta}(\psi)$ passing through the same point, i.e. $\sqrt{r_{\theta}^2(\psi) + [r'_{\theta}(\psi)]^2} / \sqrt{r_{\theta}^2(\psi) + 0^2}$.

If we define P to be the perimeter of the shape and A to be its area, then the dimensionless quantity $C = 4\pi A/P^2$ is a measure of *circularity* [8] that varies from 0 to 1. For example, circles achieve a maximum circularity of unity. Squares have circularity equal to 0.7854 and equilateral triangles have circularity 0.6046. An important feature of this measure is its scale invariance: scaling of the shape does not change its circularity measure. Recalling that $P = \int_{-\pi}^{\pi} \sqrt{r_{\theta}^2(\psi) + [r'_{\theta}(\psi)]^2} d\psi$ and $A = \frac{1}{2} \int_{-\pi}^{\pi} r_{\theta}^2(\psi) d\psi$, we can interpret the ratio $\frac{r_{\theta}(\psi)}{\sqrt{r_{\theta}^2(\psi) + [r'_{\theta}(\psi)]^2}}$ as a dimensionless measure of *instantaneous circularity* per unit ψ . Note that this measure also takes values in 0 to 1 and is invariant to scaling of shape.

C. Cramèr–Rao Bound for Infinite Dimensional Case

Let $\{B_i(\cdot)\}_{i=1}$ be a complete orthonormal basis set. Define the radial function

$$r_K(\phi) = \sum_{i=1}^K \theta_i B_i(\phi) \quad (10)$$

and its estimate

$$\hat{r}_K(\phi) = \sum_{i=1}^K \hat{\theta}_i B_i(\phi). \quad (11)$$

We make the following assumptions:

(A1) Let $r(\cdot) = \lim_{K \rightarrow \infty} r_K(\cdot)$ and $\hat{r}(\cdot) = \lim_{K \rightarrow \infty} \hat{r}_K(\cdot)$ (m.s.).

(A2) Assume that $\hat{r}(\cdot)$ is an unbiased estimate of $r(\cdot)$, with finite mean–square value (i.e. $E[\hat{r}^2(\phi)] < \infty$).

(A3) Assume that the first two derivatives of $r_K(\phi)$ and $r(\phi)$ w.r.t. ϕ exist for all ϕ and K .

Since, $E[\hat{r}^2(\phi)] < \infty$ and since the integrand and the limits of integration are finite, the estimator covariance function satisfies [34, page 180]

$$\int_{-\pi}^{\pi} \int_{-\pi}^{\pi} \text{cov}^2(\hat{r}(\phi), \hat{r}(\gamma)) d\phi d\gamma < \infty. \quad (12)$$

As the basis functions $B_1(\cdot), B_2(\cdot), \dots$ are complete and orthonormal in $[-\pi, \pi)$, we have

$$\int_{-\pi}^{\pi} B_i(\phi) B_j(\phi) d\phi = \delta_{ij} \quad (13)$$

$$\text{and } \sum_{i=1}^{\infty} \int_{-\pi}^{\pi} f(\gamma) B_i(\phi) B_i(\gamma) d\gamma = f(\phi) \quad (14)$$

where $f(\cdot)$ is any continuous function that is integrable in $[-\pi, \pi)$ and δ_{ij} is the Kronecker delta function. The former equation expresses orthonormality of the basis. The latter equation follows from the fact that $\int_{-\pi}^{\pi} f(\gamma) B_i(\gamma) d\gamma = f_i$, where f_i is the projection of $f(\cdot)$ onto the basis function $B_i(\cdot)$, and using $\sum_{i=1}^{\infty} f_i B_i(\phi) = f(\phi)$.

Define

$$h_F^K(\phi, \gamma) := C_{\text{CN}} \exp \left[-\frac{\|\vec{r}_K(\phi) - \vec{r}_K(\gamma)\|^2}{4\sigma_s^2} \right] r_K(\phi) r_K(\gamma) \quad (15)$$

$$h_F(\phi, \gamma) := C_{\text{CN}} \exp \left[-\frac{\|\vec{r}(\phi) - \vec{r}(\gamma)\|^2}{4\sigma_s^2} \right] r(\phi) r(\gamma) \quad (16)$$

$$F_{ij}^K := \iint_{-\pi}^{\pi} h_F^K(\phi, \gamma) B_i(\phi) B_j(\gamma) d\phi d\gamma. \quad (17)$$

$$\text{and } F_{ij} := \iint_{-\pi}^{\pi} h_F(\phi, \gamma) B_i(\phi) B_j(\gamma) d\phi d\gamma. \quad (18)$$

where F_{ij}^K is the Fisher information for finite dimensional case with K coefficients.

The Fisher information for this infinite dimensional case is given by the following Lemma, which is proven in Appendix A.

Lemma 1: Let the assumptions A1, A2 and A3 be satisfied. The Fisher information for the infinite dimensional case is then given by F_{ij} , where F_{ij}^K uniformly converges to F_{ij} as $K \rightarrow \infty$. Furthermore,

$$\sum_{i=1}^{\infty} F_{ii} \leq C_{\text{CN}} \int_{-\pi}^{\pi} r^2(\phi) d\phi. \quad (19)$$

□

Define the following 2 additional conditions

(A4) Suppose there exists G_{ij} such that

$$\sum_{l=1}^{\infty} G_{il} F_{lj} = \sum_{l=1}^{\infty} F_{il} G_{lj} = \delta_{ij}. \quad (20)$$

(A5) For any square summable sequence $\{x_i\}_{i=1}^{\infty}$, assume that the covariance of $\hat{\theta}_i$ satisfies

$$\sum_{i=1}^{\infty} \sum_{j=1}^{\infty} x_i \text{cov}(\hat{\theta}_i, \hat{\theta}_j) x_j \geq \sum_{i=1}^{\infty} \sum_{j=1}^{\infty} x_i G_{ij} x_j. \quad (21)$$

If both (A4) and (A5) are satisfied, then by definition, G_{ij} is the CR bound on the covariance of $\hat{\theta}_i$. Note that if either one of (A4) and (A5) fail to hold, then the determination of the infinite dimensional CR bound is an open problem.

If both (A4) and (A5) are satisfied, then a restricted CR bound for infinite dimensional case can be obtained from the following Lemma, which is proven in Appendix B.

Lemma 2: Let the assumptions A1, A2, A3, and A5 be satisfied. Suppose there exists an integrable function $h_G(\cdot, \cdot)$ that satisfies

$$\int_{-\pi}^{\pi} h_F(\phi, \psi) h_G(\psi, \gamma) d\psi = \delta(\phi, \gamma). \quad (22)$$

i.e. $h_G(\cdot, \cdot)$ is the operator inverse of $h_F(\cdot, \cdot)$. Then

$$G_{ij} := \iint_{-\pi}^{\pi} h_G(\phi, \gamma) B_i(\phi) B_j(\gamma) d\phi d\gamma \quad (23)$$

satisfies (20). Hence A4 is satisfied. From assumption (A5), the covariance of $\hat{r}(\phi)$ satisfies

$$\text{cov}(\hat{r}(\phi), \hat{r}(\gamma)) - h_G(\phi, \gamma) \text{ is n.n.d.}$$

□

D. Best–Shape Analysis for Finite Dimensional Case

We need the following Lemma, which is proven in Appendix C.

Lemma 3: Assume that the derivatives r' , r'' , r''' exist and are finite. The only star–shaped object that satisfies

$$\frac{r^2(\psi)}{\sqrt{r^2(\psi) + [r'(\psi)]^2}} = c, \quad \forall \psi \quad (24)$$

where c is a constant, is a circular disk. □

This allows us to establish the optimality of the disk shapes

Theorem 3.1: Let K be finite and define \mathcal{S}_K the set of shapes having boundary function $r(\phi)$ in the linear span of the basis $\{\phi_i\}_{i=1}^K$. If \mathcal{S}_K contains the class of disk shapes then, to order $o(\sigma_m)$, the maximum eigenvalue of the Cramèr–Rao bound is minimized over \mathcal{S}_K by this class of shapes. □

Proof of Theorem 3.1:

The asymptotic form for the Fisher information matrix is given by [11]

$$\mathbf{F}_\theta = \frac{(\text{contrast})^2}{2\sqrt{\pi}\sigma_s\sigma_n^2} \int_{-\pi}^{\pi} h_\theta(\psi) \mathbf{B}(\psi)\mathbf{B}^T(\psi)d\psi + o(\sigma_m). \quad (25)$$

Let \mathbf{x} be any K -dimensional vector such that $\mathbf{x}^T\mathbf{x} = 1$. Then an upper bound on the maximum eigenvalue of \mathbf{F}_θ is obtained as follows

$$\begin{aligned} \mathbf{x}^T\mathbf{F}_\theta\mathbf{x} &= \frac{(\text{contrast})^2}{2\sqrt{\pi}\sigma_s\sigma_n^2} \int_{-\pi}^{\pi} h_\theta(\psi) (\mathbf{x}^T\mathbf{B}(\psi))^2 d\psi + o(\sigma_m) \\ &\leq \max_{\psi} h_\theta(\psi) \frac{(\text{contrast})^2}{2\sqrt{\pi}\sigma_s\sigma_n^2} \int_{-\pi}^{\pi} (\mathbf{x}^T\mathbf{B}(\psi))^2 d\psi + o(\sigma_m) \end{aligned}$$

with equality if and only if

$$h_\theta(\psi) = \frac{r_\theta^2(\psi)}{\sqrt{r_\theta^2(\psi) + [r'_\theta(\psi)]^2}} = c, \quad \forall \psi \in [-\pi, \pi),$$

for some positive constant c independent of ψ . From Lemma 3 this is true only for a disk. Thus, as the maximum eigenvalue of \mathbf{F}_θ is identical to the minimum eigenvalue of the CR bound on the covariance matrix, the Theorem follows. ■

E. Worst–Shape Analysis for Finite Dimensional Case

Here we explore shapes which minimize the trace of the asymptotic Fisher information matrix (25):

$$\text{trace}\{\mathbf{F}_\theta\} = C \int_{\phi=-\pi}^{\pi} h_\theta(\phi) f_B(\phi) d\phi \quad (26)$$

where $C = \frac{(\text{contrast})^2}{2\sqrt{\pi}\sigma_s\sigma_n^2}$ and

$$f_B(\phi) = \mathbf{B}^T(\phi)\mathbf{B}(\phi) = \sum_{i=1}^K B_i^2(\phi).$$

Since, by Schwarz's inequality, for any K –dimensional symmetric positive definite matrix \mathbf{A} , $\text{trace}\{\mathbf{A}^{-1}\} \geq K/\text{trace}\{\mathbf{A}\}$, $K/\text{trace}\{\mathbf{F}_\theta\} \leq \text{trace}\{\mathbf{F}_\theta^{-1}\}$. Hence minimizing the trace of \mathbf{F}_θ maximizes a lower bound on the trace of the CR bound.

First we used numerical methods (constrained gradient search) to find shapes, specifically $r_\theta(\phi)$ in the class of B–splines with K equally spaced knots, which minimize $\text{trace}\{\mathbf{F}_\theta\}$ subject to the fixed perimeter constraint

$$P = \int_{\phi=-\pi}^{\pi} \sqrt{[r_\theta(\phi)]^2 + [r'_\theta(\phi)]^2} d\phi = 1. \quad (27)$$

The worst–case shapes found by numerical optimization are shown in Figure 2. Each of these shapes is a rhodonea (rose shaped) curve [35] with a number of petals equal to one half the number of knots (K =even).

The global worst–case shapes in Figure 2 represent extreme deviations from circularity which for many applications may not be frequently encountered in practice. To explore the sensitivity of the Fisher information over a more representative set of shapes we investigated worst–case shapes over the class of nearly circular shapes whose boundary functions $r_\theta(\phi)$ satisfy both the perimeter constraint (27) and the circularity constraint:

$$\frac{4\pi A}{P^2} = \frac{4\pi \int_{\phi=-\pi}^{\pi} r_\theta^2(\phi) d\phi}{\left(\int_{\phi=-\pi}^{\pi} \sqrt{[r_\theta(\phi)]^2 + [r'_\theta(\phi)]^2} d\phi \right)^2} \geq \gamma \quad (28)$$

where $\gamma \in [0, 1]$ is a specified circularity parameter close to one. As the circle maximizes enclosed area among all closed curves of fixed perimeter, the left hand side of the inequality in (28) takes on its maximum value of unity when r_θ corresponds to a disk shape, i.e. $\theta = \mathbf{1} = [1, \dots, 1]^T$ [9, Thm. 4.5].

Under the assumption that γ close to one, a second order Taylor development about $\theta = \mathbf{1}$ yields the following local approximation to the left hand side of the perimeter constraint (27)

$$\int_{\phi=-\pi}^{\pi} \sqrt{[r_\theta(\phi)]^2 + [r'_\theta(\phi)]^2} d\phi = \mathbf{a}^T \theta + \frac{1}{2} \theta^T \mathbf{D} \theta + o(\|\theta - \mathbf{1}\|^2)$$

and the local approximation to the trace of the Fisher information (26)

$$\text{trace}\{\mathbf{F}_\theta\} = C(\mathbf{a}_f^T \boldsymbol{\theta} - \frac{1}{2} \boldsymbol{\theta}^T \mathbf{D}_f \boldsymbol{\theta}) + o(\|\boldsymbol{\theta} - \mathbf{1}\|^2)$$

where

$$\mathbf{a} = \int_{\phi=-\pi}^{\pi} \mathbf{B}(\phi) d\phi \quad (29)$$

$$\mathbf{a}_f = \int_{\phi=-\pi}^{\pi} \mathbf{B}(\phi) f_B(\phi) d\phi \quad (30)$$

$$\mathbf{D} = \int_{\phi=-\pi}^{\pi} \mathbf{B}'(\phi) [\mathbf{B}'(\phi)]^T d\phi \quad (31)$$

$$\mathbf{D}_f = \int_{\phi=-\pi}^{\pi} \mathbf{B}'(\phi) [\mathbf{B}'(\phi)]^T f_B(\phi) d\phi, \quad (32)$$

and \mathbf{B}' denotes the vector of first derivatives of the basis elements $B_i(\phi)$ with respect to ϕ . Furthermore, under the perimeter constraint, the circularity constraint reduces to $4\pi \boldsymbol{\theta}^T \mathbf{Q} \boldsymbol{\theta} \geq \gamma$ where

$$\mathbf{Q} = \int_{\phi=-\pi}^{\pi} \mathbf{B}(\phi) \mathbf{B}^T(\phi) d\phi$$

Therefore, by forcing γ to be close to one the problem of minimization over $\boldsymbol{\theta}$ of the trace of the Fisher information subject to the perimeter and circularity constraints is approximately quadratic in $\boldsymbol{\theta}$ with associated Lagrangian

$$L(\boldsymbol{\theta}) = \mathbf{a}_f^T \boldsymbol{\theta} - \frac{1}{2} \boldsymbol{\theta}^T \mathbf{D}_f \boldsymbol{\theta} + \lambda_1 \boldsymbol{\theta}^T \mathbf{Q} \boldsymbol{\theta} + \lambda_2 (\mathbf{a}^T \boldsymbol{\theta} + \frac{1}{2} \boldsymbol{\theta}^T \mathbf{D} \boldsymbol{\theta})$$

where λ_1 and λ_2 are undetermined multipliers selected so as to satisfy the local perimeter and circularity constraints jointly expressed as

$$P = \mathbf{a}^T \boldsymbol{\theta} + \frac{1}{2} \boldsymbol{\theta}^T \mathbf{D} \boldsymbol{\theta} = 1 \quad (33)$$

$$A = \boldsymbol{\theta}^T \mathbf{Q} \boldsymbol{\theta} = \gamma / (4\pi). \quad (34)$$

Using a K -dimensional subset of the quadratic B-spline basis functions $\mathbf{B}(\phi)$, the plot of $f_{\mathbf{B}}(\cdot)$ for various number K of knots is given in Figure 3. The corresponding worst-shapes local to circle ($\gamma = 0.9$) are shown in Figure 4 and exhibit characteristic flower shaped boundaries.

F. Best-Shape Analysis for Infinite Dimensional Case

We refer to (19) of Lemma 1 for the relation between sum of F_{ii} over all i and the total area of the shape, recalling that area = $\int_{-\pi}^{\pi} r^2(\phi) d\phi$. For a fixed perimeter, the area is maximized for a circle. Hence, circular disks are again

estimated with most confidence. So, for both finite and infinite dimensional cases, circular disks are estimated with least error.

G. Worst–Shape Analysis for Infinite Dimensional Case

We refer to Lemma 1. From (19), we see that the uncertainty of $\hat{\theta}_i$ increases for shapes with smaller area. A smaller area is achieved for a fixed perimeter when there are sharp and narrow spikes on the shape. The area is minimized when $r(\phi)$ is very close to zero for all ϕ . Since there is a constraint on perimeter, we conjecture that $r(\phi)$ will have sharp spikes, uniformly spread along $\phi \in [-\pi, \pi)$ in such a way that the perimeter constraint is met.

IV. OPTIMUM CENTER–OF–DESCRIPTION FOR 2D SHAPE ESTIMATION

As mentioned earlier, the choice of center–of–description is an important issue. For example, suppose we are estimating circular shapes, if the center–of–description is the geometric center of the circular shape, then estimation error will be minimum, as we saw earlier. However, if the center–of–description is on the boundary or very close to the boundary of the circular shape, then estimation error will be greater. In this section, we show an approach to find optimum center. The optimum center can be found using the Fisher information for finite or infinite dimensional cases. For concreteness we focus on the infinite dimensional case.

A. Set up of Problem

We assume that a description $r(\phi)$ of the boundary is known with respect to a known center O as in Figure 5. Let \tilde{O} be a new center–of–description so that the same object can be described by $\tilde{r}(\phi)$, where the angle ϕ is with respect to the previous origin O . Recall from Lemma 1, we have $\sum_{i=1}^{\infty} F_{ii} \leq C_{CN} \int_{-\pi}^{\pi} r^2(\phi) d\phi$. So, we can maximize a bound on the trace of the \mathbf{F}_{θ} over shape by maximizing

$$f = \int_{-\pi}^{\pi} r^2(\phi) d\phi. \quad (35)$$

Let the new center \tilde{O} be located at (r_c, ϕ_c) with respect to O . This is shown in Figure 5. Now, using a trigonometric equality,

$$\tilde{r}_{\tilde{\theta}}^2(\phi) = r_c^2 + r^2(\phi) - 2r_c r(\phi) \cos(\phi_c - \phi).$$

Define the function

$$\tilde{f}(r_c, \phi_c) = \int_{-\pi}^{\pi} \tilde{r}^2(\phi) d\phi$$

$$= \int_{-\pi}^{\pi} [r_c^2 + r^2(\phi) - 2r_c r(\phi) \cos(\phi_c - \phi)] d\phi. \quad (36)$$

In order to locate an optimum center, we should maximize the function $\tilde{f}(r_c, \phi_c)$ with respect to r_c and ϕ_c .

B. Determining Optimum Center-of-Description

To minimize $\tilde{f}(r_c, \phi_c)$ with respect to r_c and ϕ_c , the necessary conditions are given by

$$\frac{\partial \tilde{f}}{\partial r_c} = 0 \implies r_c = \frac{1}{2\pi} \int_{-\pi}^{\pi} r(\phi) \cos(\phi_c - \phi) d\phi \quad (37)$$

$$\text{and } \frac{\partial \tilde{f}}{\partial \phi_c} = 0 \implies \int_{-\pi}^{\pi} r(\phi) \sin(\phi_c - \phi) d\phi = 0. \quad (38)$$

Observe from (37) and (38) that the optimum center is not necessarily the centroid. An analogous procedure can be used for the finite dimensional case to determine optimum center-of-description.

C. Sensitivity of CR bound to Center-of-Description

To see how the center-of-description affects the trace of asymptotic CR bound, we performed two experiments: one with a circle and the other with a test shape. We shifted the center-of-description for these two shapes and evaluated the trace of asymptotic CR bound in (7). Because of the symmetry of the circle, for the former case we shifted the center-of-description along a fixed angle radial segment. The plot of the trace of the asymptotic CR bound against radial shift of center-of-description for a circle of radius 5 units is shown in Figure 6. Observe that the optimum position of the center-of-description is at the centroid, i.e. geometric center of the disc. Note that the trace of CR bound is not monotonic, it starts to decrease when the center-of-description approaches the boundary. This is due to the trade-off between the value of $h_{\theta}(\psi)$ for boundary points close to the center-of-description and boundary points away from the center-of-description. This trade-off depends on the shape in general. Thus, for the circle of radius 5 units, the peak of trace bound occurs for a shift less than 5 units.

Figure 7 shows a test object for the second experiment. The area marked by dotted lines is the region of center-of-description locations for which the shape can be described as a star-shape. The figure shows the shape centroid, optimum center and worst center. The optimum center and worst center were found using exhaustive search. This is an example where the centroid is not the optimum center-of-description. The best center appears to be the center-of-description that maximizes the minimum distance to boundary. Also note that the worst center for this test shape lies on the boundary of the region marked by dotted lines, i.e. at the limit of the center-of-description for which the object can be described as star-shaped.

V. 3D SHAPE ESTIMATION

In this section, we extend the finite dimensional results for 2D shape estimation. The infinite dimensional extension is not treated here. We follow a similar procedure to derive the Fisher information and its asymptotic expression. The model for uncorrupted 3D image is

$$I_{\hat{\theta}}(x, y, z) = C_{\text{INT}} \cdot I_{R_{\hat{\theta}}}(x, y, z) + C_{\text{BG}} \cdot (1 - I_{R_{\hat{\theta}}}(x, y, z)). \quad (39)$$

The model for observed data is

$$Y_{\text{M}}(x, y, z) = (I_{\hat{\theta}} * * * H)(x, y, z) + n(x, y, z) \quad (40)$$

where $* * *$ denotes three-dimensional convolution. As in the 2D case we assume that the point spread function $H(\cdot, \cdot, \cdot)$ is spatial invariant symmetric Gaussian with blur parameter σ_s , and noise $n(\cdot, \cdot, \cdot)$ is zero mean white Gaussian with power spectral density σ_n^2 . Again, we focus on star-shapes. The radius $r_{\theta}(\alpha, \beta)$ is described as a function of angle of elevation α and angle of azimuth β as defined in Figure 8, where θ is a vector of basis coefficients. Similarly to the 2D case, the basis functions can be represented in vector form as $B_i(\alpha, \beta)$ and $\mathbf{B}(\alpha, \beta) = [B_1(\alpha, \beta), B_2(\alpha, \beta), \dots, B_K(\alpha, \beta)]^T$. As an explicit example, tensor spline model represents the radius function as a tensor product

$$r_{\theta}(\alpha, \beta) = \sum_{i=1}^{K_{el}} \sum_{j=1}^{K_{az}} \theta_{ij} B_i^{el}(\alpha) B_j^{az}(\beta) \quad (41)$$

where $B_i^{el}(\cdot)$ and $B_j^{az}(\cdot)$ are basis functions along axes for elevation and azimuth angles, respectively. Alternatively, this representation can be rearranged lexicographically to obtain a more general form:

$$r_{\theta}(\alpha, \beta) = \sum_{i=1}^K \theta_i B_i(\alpha, \beta). \quad (42)$$

A. Fisher Information for 3D Shape

An expression for Fisher information is given in the following Lemma, whose proof is in Appendix D.

Lemma 4: The Fisher information \mathbf{F}_{θ} for parametric estimation of 3 Dimensional shapes is given by

$$\mathbf{F}_{\theta} = C_{\text{CN}} \cdot \int_{\alpha_1=-\frac{\pi}{2}}^{\frac{\pi}{2}} \int_{\beta_1=-\pi}^{\pi} \int_{\alpha_2=-\frac{\pi}{2}}^{\frac{\pi}{2}} \int_{\beta_2=-\pi}^{\pi} \exp\left(\frac{\|\vec{r}_{\theta}(\alpha_1, \beta_1) - \vec{r}_{\theta}(\alpha_2, \beta_2)\|^2}{-4\sigma_s^2}\right) r_{\hat{\theta}}^2(\alpha_1, \beta_1) r_{\hat{\theta}}^2(\alpha_2, \beta_2) \cdot \mathbf{B}(\alpha_1, \beta_1); \mathbf{B}^T(\alpha_2, \beta_2) \cos \alpha_1 \cos \alpha_2 d\alpha_1 d\beta_1 d\alpha_2 d\beta_2 \quad (43)$$

where

$$C_{\text{CN}} := \frac{(C_{\text{INT}} - C_{\text{BG}})^2}{8\pi^{3/2}\sigma_s^3\sigma_n^2} = \frac{\text{contrast}^2}{8\pi^{3/2}\sigma_s^3\sigma_n^2}. \quad \square$$

This expression is similar to the Fisher information for 2D case in (6). In the following Lemma, we give an asymptotic expression for \mathbf{F}_θ . This Lemma is proven in Appendix E.

Lemma 5: Assume $r_\theta(\alpha, \beta) > 0$ and $r_\theta(\alpha, \beta), r_\theta^{10}(\alpha, \beta), r_\theta^{01}(\alpha, \beta), r_\theta^{11}(\alpha, \beta), r_\theta^{20}(\alpha, \beta)$ and $r_\theta^{02}(\alpha, \beta)$ are bounded for all $\alpha \in [-\pi/2, \pi/2]$ and $\beta \in [-\pi, \pi]$. The superscripts 10, 01, 11, 20 and 02 are short-hand notation for the partial derivatives $\frac{\partial}{\partial \alpha}, \frac{\partial}{\partial \beta}, \frac{\partial^2}{\partial \alpha \partial \beta}, \frac{\partial^2}{\partial \alpha^2}$ and $\frac{\partial^2}{\partial \beta^2}$ respectively. Then

$$\mathbf{F}_\theta = 4\pi C_{\text{CN}} \sigma_s^2 \int_{\alpha=-\frac{\pi}{2}}^{\frac{\pi}{2}} \int_{\beta=-\pi}^{\pi} h_\theta(\alpha, \beta) \mathbf{B}(\alpha, \beta) \mathbf{B}^T(\alpha, \beta) \cos^2 \alpha d\alpha d\beta + o(\sigma_m) \quad (44)$$

where

$$h_\theta(\alpha, \beta) := \frac{r_\theta^4(\alpha, \beta)}{\sqrt{\|\vec{r}_\theta^{10}(\alpha, \beta)\|^2 \|\vec{r}_\theta^{01}(\alpha, \beta)\|^2 - \langle \vec{r}_\theta^{10}(\alpha, \beta), \vec{r}_\theta^{01}(\alpha, \beta) \rangle^2}} \quad (45)$$

$$\rho_\theta(\alpha, \beta) := \frac{\langle \vec{r}_\theta^{10}(\alpha, \beta), \vec{r}_\theta^{01}(\alpha, \beta) \rangle}{\|\vec{r}_\theta^{10}(\alpha, \beta)\| \|\vec{r}_\theta^{01}(\alpha, \beta)\|} \quad (46)$$

$$\sigma_1(\alpha, \beta) := \frac{\sqrt{2}\sigma_s}{\|\vec{r}_\theta^{10}(\alpha, \beta)\| \sqrt{1 - \rho_\theta^2(\alpha, \beta)}} \quad (47)$$

$$\sigma_2(\alpha, \beta) := \frac{\sqrt{2}\sigma_s}{\|\vec{r}_\theta^{01}(\alpha, \beta)\| \sqrt{1 - \rho_\theta^2(\alpha, \beta)}} \quad (48)$$

$$\text{and } \sigma_m := \max_{\alpha, \beta} \frac{\sigma_1(\alpha, \beta) + \sigma_2(\alpha, \beta)}{2}. \quad (49)$$

□

Again, this expression is similar to the asymptotic expression for 2D case in (25). We define $\|\vec{r}_\theta^{10}(\alpha, \beta)\|$ to be the speed of the differential surface element shown in Figure 8 along the axis of elevation. Similarly, $\|\vec{r}_\theta^{01}(\alpha, \beta)\|$ is the speed of differential surface element along the axis of azimuth. ρ_θ is the linear correlation coefficient between the elevation and azimuth components of the radial gradient field and σ_m is the maximum of average resolution-speed ratio along elevation and azimuth axes. Note the similarity between σ_m for the 2D case as in (9).

B. Interpretation of $h_\theta(\alpha, \beta)$

The reader is referred to Figure 8. Let O be the center-of-description for the shape represented by $r_\theta(\alpha, \beta)$. Let P be a point on the surface. Let $\vec{OP} = x \hat{i} + y \hat{j} + z \hat{k}$, where \hat{i}, \hat{j} and \hat{k} are unit vectors along X, Y and Z axes respectively. Hence,

$$\begin{aligned} \vec{r}_\theta(\alpha, \beta) &= \vec{OP} = r_\theta(\alpha, \beta) \left[\cos \alpha \cos \beta \hat{i} + \cos \alpha \sin \beta \hat{j} + \sin \alpha \hat{k} \right] \\ \vec{r}_\theta^{10}(\alpha, \beta) &= \frac{r_\theta^{10}(\alpha, \beta) \vec{r}_\theta(\alpha, \beta)}{r_\theta(\alpha, \beta)} + r_\theta(\alpha, \beta) \left[-\sin \alpha \cos \beta \hat{i} - \sin \alpha \sin \beta \hat{j} + \cos \alpha \hat{k} \right] \end{aligned} \quad (50)$$

and (51)

$$\vec{r}_{\theta}^{01}(\alpha, \beta) = \frac{r_{\theta}^{01}(\alpha, \beta) \vec{r}_{\theta}(\alpha, \beta)}{r_{\theta}(\alpha, \beta)} + r_{\theta}(\alpha, \beta) \left[-\cos \alpha \sin \beta \hat{i} - \cos \alpha \cos \beta \hat{j} + \cos \alpha \hat{k} \right] \quad (52)$$

Define

$$\vec{t}_1 := -\sin \alpha \cos \beta \hat{i} - \sin \alpha \sin \beta \hat{j} + \cos \alpha \hat{k} \quad (53)$$

$$\vec{t}_2 := -\cos \alpha \sin \beta \hat{i} - \cos \alpha \cos \beta \hat{j} + \cos \alpha \hat{k} \quad (54)$$

$$\text{and } \vec{n} := \cos \alpha \cos \beta \hat{i} + \cos \alpha \sin \beta \hat{j} + \sin \alpha \hat{k}. \quad (55)$$

Then

$$\vec{r}_{\theta}^{10}(\alpha, \beta) = r_{\theta}^{10}(\alpha, \beta) \vec{n} + r_{\theta}(\alpha, \beta) \vec{t}_1 \quad (56)$$

$$\vec{r}_{\theta}^{01}(\alpha, \beta) = r_{\theta}^{01}(\alpha, \beta) \vec{n} + r_{\theta}(\alpha, \beta) \vec{t}_2. \quad (57)$$

Note that \vec{t}_1, \vec{t}_2 and \vec{n} are unit vectors and are mutually orthogonal. Thus, we have decomposed $\vec{r}_{\theta}^{10}(\alpha, \beta)$ and $\vec{r}_{\theta}^{01}(\alpha, \beta)$ into weighted sum of mutually orthogonal unit vectors. Consider a spherical surface passing through P with O as its center, as shown in Figure 8. Then the unit vectors \vec{t}_1 and \vec{t}_2 span the tangent space at P for the sphere, and \vec{n} is a normal vector to the sphere at P . Thus

$$\|\vec{r}_{\theta}^{10}(\alpha, \beta)\|^2 = [r_{\theta}^{10}(\alpha, \beta)]^2 + r_{\theta}^2(\alpha, \beta) \quad (58)$$

$$\|\vec{r}_{\theta}^{01}(\alpha, \beta)\|^2 = [r_{\theta}^{01}(\alpha, \beta)]^2 + r_{\theta}^2(\alpha, \beta) \quad (59)$$

and

$$\langle \vec{r}_{\theta}^{10}(\alpha, \beta), \vec{r}_{\theta}^{01}(\alpha, \beta) \rangle = r_{\theta}^{10}(\alpha, \beta) r_{\theta}^{01}(\alpha, \beta) \quad (60)$$

$$\vec{r}_{\theta}^{10}(\alpha, \beta) \times \vec{r}_{\theta}^{01}(\alpha, \beta) = r_{\theta}^{10}(\alpha, \beta) r_{\theta}(\alpha, \beta) \vec{t}_1 + r_{\theta}^{01}(\alpha, \beta) r_{\theta}(\alpha, \beta) \vec{t}_2 + r_{\theta}^2(\alpha, \beta) \vec{n}. \quad (61)$$

Recall that if \vec{a} and \vec{b} are the adjacent sides of a parallelogram, then $\|\vec{a} \times \vec{b}\|$ is its area. Also, $\|\vec{a} \times \vec{b}\|^2 = \|\vec{a}\|^2 \|\vec{b}\|^2 - \langle \vec{a}, \vec{b} \rangle^2$. The denominator (45) of $h_{\theta}(\alpha, \beta)$ is thus the area of the parallelogram determined by $\vec{r}_{\theta}^{10}(\alpha_2, \beta_2)$ and $\vec{r}_{\theta}^{01}(\alpha_2, \beta_2)$.

Note that $\vec{r}_{\theta}^{10}(\alpha, \beta)$ and $\vec{r}_{\theta}^{01}(\alpha, \beta)$ lie in the tangent plane of the surface $r_{\theta}(\alpha, \beta)$ at P and $\vec{r}_{\theta}^{10}(\alpha, \beta) \times \vec{r}_{\theta}^{01}(\alpha, \beta)$ gives the direction of the normal at P . Thus the distance between the tangent plane from the center O is given by the

projection of \vec{OP} on the unit normal vector. Using (61), this is given by

$$\begin{aligned} & \frac{\langle \vec{OP}, \vec{r}_{\theta}^{10}(\alpha, \beta) \times \vec{r}_{\theta}^{01}(\alpha, \beta) \rangle}{\|\vec{r}_{\theta}^{10}(\alpha, \beta) \times \vec{r}_{\theta}^{01}(\alpha, \beta)\|} \\ &= \frac{\langle r_{\theta}(\alpha, \beta) \vec{n}, r_{\theta}^{10}(\alpha, \beta) r_{\theta}(\alpha, \beta) \vec{t}_1 + r_{\theta}^{01}(\alpha, \beta) r_{\theta}(\alpha, \beta) \vec{t}_2 + r_{\theta}^2(\alpha, \beta) \vec{n} \rangle}{\|\vec{r}_{\theta}^{10}(\alpha, \beta) \times \vec{r}_{\theta}^{01}(\alpha, \beta)\|} \\ &= \frac{r_{\theta}^3(\alpha, \beta)}{\|\vec{r}_{\theta}^{10}(\alpha, \beta) \times \vec{r}_{\theta}^{01}(\alpha, \beta)\|}. \end{aligned}$$

since \vec{t}_1, \vec{t}_2 and \vec{n} are mutually orthogonal unit vectors.

Thus, $h_{\theta}(\alpha, \beta)$ is the product of distance of point P on surface located at angle (α, β) from the center O and the distance of tangent plane at P from O . Using (61),

$$h_{\theta}(\alpha, \beta) = \frac{r_{\theta}^3(\alpha, \beta)}{\sqrt{[r_{\theta}^{10}(\alpha, \beta)]^2 + [r_{\theta}^{01}(\alpha, \beta)]^2 + r_{\theta}^2(\alpha, \beta)}}. \quad (62)$$

Similarly, we get

$$\rho_{\theta}(\alpha, \beta) = \frac{r_{\theta}^{10}(\alpha, \beta) r_{\theta}^{01}(\alpha, \beta)}{\sqrt{[r_{\theta}^{10}(\alpha, \beta)]^2 + r_{\theta}^2(\alpha, \beta)} \sqrt{[r_{\theta}^{01}(\alpha, \beta)]^2 + r_{\theta}^2(\alpha, \beta)}} \quad (63)$$

$$\sigma_1(\alpha, \beta) = \frac{\sqrt{2} \sigma_s \sqrt{[r_{\theta}^{01}(\alpha, \beta)]^2 + r_{\theta}^2(\alpha, \beta)}}{r_{\theta}(\alpha, \beta) \sqrt{[r_{\theta}^{10}(\alpha, \beta)]^2 + [r_{\theta}^{01}(\alpha, \beta)]^2 + r_{\theta}^2(\alpha, \beta)}} \quad (64)$$

$$\sigma_2(\alpha, \beta) = \frac{\sqrt{2} \sigma_s \sqrt{[r_{\theta}^{10}(\alpha, \beta)]^2 + r_{\theta}^2(\alpha, \beta)}}{r_{\theta}(\alpha, \beta) \sqrt{[r_{\theta}^{10}(\alpha, \beta)]^2 + [r_{\theta}^{01}(\alpha, \beta)]^2 + r_{\theta}^2(\alpha, \beta)}} \quad (65)$$

We can write $h_{\theta}(\alpha, \beta)$ as a ratio of $r_{\theta}^2(\alpha, \beta)$ (same dimensions as area) and the dimensionless quantity

$$\sqrt{1 + \left[\frac{r_{\theta}^{10}(\alpha, \beta)}{r_{\theta}(\alpha, \beta)} \right]^2 + \left[\frac{r_{\theta}^{01}(\alpha, \beta)}{r_{\theta}(\alpha, \beta)} \right]^2}.$$

The dimensionless quantity is also the ratio of speed of the surface at (α, β) to the speed of spherical surface of radius $r_{\theta}(\alpha, \beta)$ passing through the same point. This quantity will be called the instantaneous sphericity of the 3D object and is analogous to the measure of circularity which characterized the CR bound for the case of 2D objects.

C. Extremal Shape Analysis

Since the form of the asymptotic 2D and 3D Fisher information matrices are very similar an analog to Theorem 3.1 is easily shown: the sphere is the optimum 3D shape.

Similarly to the 2D case studied previously, we can explore worst-shapes by employing numerical minimization of the trace of the Fisher matrix subject to the surface area constraint

$$S = \int_{\alpha=-\pi/2}^{\pi/2} \int_{\beta=-\pi}^{\pi} \sqrt{[r_{\boldsymbol{\theta}}(\alpha, \beta)]^2 + [r_{\boldsymbol{\theta}^{10}}(\alpha, \beta)]^2 + [r_{\boldsymbol{\theta}^{01}}(\alpha, \beta)]^2} r_{\boldsymbol{\theta}}(\alpha, \beta) \cos(\alpha) d\alpha d\beta = 1. \quad (66)$$

For the numerical studies we used a tensor quadratic B-spline basis with equal number of equally spaced knots for both the azimuth and elevation basis sets. In Figs. 9-10 we show 4 different views of the worst-shapes for 3×3 and 4×4 knots in the tensor bases, respectively. The knot positions are indicated by light colored boxes. These worst case shapes are not necessarily unique but indicate that highly non-convex star-shaped objects are hardest to estimate. Note, as in the 2D case, for each of these shapes the set of valid choices of center-of-description reduces to a single point at one of the knot positions.

Using a completely analogous analysis as presented for the 2D case a worst case analysis of shapes local to the sphere can be performed under the additional sphericity constraint $36\pi V^2/S^3 \geq \gamma$ where S and V are the surface area and volume of the shape, respectively, and $\gamma \in [0, 1]$ is close to unity. The sphericity measure on the left hand side of this constraint inequality takes on its maximum value of unity for a sphere [9, p. 289]. The local Lagrangian for this case reduces to the quadratic objective:

$$L(\boldsymbol{\theta}) = \boldsymbol{\theta}^T [\mathbf{Q}_f - \frac{1}{2}\mathbf{D}_f] \boldsymbol{\theta} + \lambda_1 (\boldsymbol{\theta}^T \mathbf{Q} \boldsymbol{\theta} - \mathbf{a}^T \boldsymbol{\theta}) + \lambda_2 (\frac{1}{2}\boldsymbol{\theta}^T [\mathbf{D} + \mathbf{Q}] \boldsymbol{\theta} + \mathbf{a}^T \boldsymbol{\theta})$$

where, now

$$\begin{aligned} \mathbf{a} &= \int_{\alpha=-\pi/2}^{\pi/2} \int_{\beta=-\pi}^{\pi} \mathbf{B}(\alpha, \beta) \cos(\alpha) d\alpha d\beta \\ \mathbf{Q} &= \int_{\alpha=-\pi/2}^{\pi/2} \int_{\beta=-\pi}^{\pi} \mathbf{B}(\alpha, \beta) \mathbf{B}^T(\alpha, \beta) \cos(\alpha) d\alpha d\beta \\ \mathbf{Q}_f &= \int_{\alpha=-\pi/2}^{\pi/2} \int_{\beta=-\pi}^{\pi} \mathbf{B}(\alpha, \beta) \mathbf{B}^T(\alpha, \beta) f_B(\alpha, \beta) \cos^2(\alpha) d\alpha d\beta \\ \mathbf{D} &= \int_{\alpha=-\pi/2}^{\pi/2} \int_{\beta=-\pi}^{\pi} [\mathbf{B}_{10}(\alpha, \beta) \mathbf{B}_{10}^T(\alpha, \beta) + \mathbf{B}_{01}(\alpha, \beta) \mathbf{B}_{01}^T(\alpha, \beta)] \cos(\alpha) d\alpha d\beta \\ \mathbf{D}_f &= \int_{\alpha=-\pi/2}^{\pi/2} \int_{\beta=-\pi}^{\pi} [\mathbf{B}_{10}(\alpha, \beta) \mathbf{B}_{10}^T(\alpha, \beta) + \mathbf{B}_{01}(\alpha, \beta) \mathbf{B}_{01}^T(\alpha, \beta)] f_B(\alpha, \beta) \cos^2(\alpha) d\alpha d\beta \end{aligned}$$

and λ_1 and λ_2 are selected to ensure the constraints

$$\begin{aligned} S &= \frac{1}{2} \boldsymbol{\theta}^T \mathbf{D} \boldsymbol{\theta} + \frac{1}{2} (\boldsymbol{\theta}^T \mathbf{Q} \boldsymbol{\theta} - 1) + \mathbf{a}^T \boldsymbol{\theta} = 1 \\ V &= \boldsymbol{\theta}^T \mathbf{Q} \boldsymbol{\theta} - \mathbf{a}^T \boldsymbol{\theta} + 4/3 \pi = \sqrt{\gamma/36\pi}, \end{aligned}$$

and $\mathbf{B}_{10}(\alpha, \beta)$ and $\mathbf{B}_{01}(\alpha, \beta)$ denote vectors of partial derivatives of $\mathbf{B}(\alpha, \beta)$ with respect to α and β , respectively.

The local worst–shapes for tensor quadratic B–splines are shown in Figure 11 for 3×3 , 4×4 , 8×8 and 12×12 knots. Similarly to the 2D case these worse case shapes have oscillating surfaces where the period of oscillation is determined by the number and placement of the knots.

VI. CONCLUSIONS

We have analyzed the performance of parametric estimators of boundaries of 2D and 3D star–shaped objects using the CR bound and Fisher information. Asymptotic expressions for Fisher information for both 2D and 3D shapes were presented and similarities between them were observed. Our results predict that estimation accuracy depends on the circularity (2D) or sphericity (3D) of the boundary of the underlying shape as measured by the speed of the curve (2D) or surface (3D). We showed that circles and spheres are the shapes which are easiest to accurately estimate in that they minimize the maximum eigenvalue of the CR bound. We also showed that for quadratic B–splines flower–shaped objects are the hardest to estimate in that they minimize the trace of the Fisher information matrix.

APPENDIX

I. PROOF OF LEMMA 1 (UNCONSTRAINED FISHER INFORMATION FOR 2D SHAPE)

The Fisher information F_{ij}^K for finite dimensional case can be obtained from (6). So, we get (17) directly. By assumption A3, $r_K(\phi)$ and $dr_K(\phi)/d\phi$ exist for all ϕ and K . Note that $h_F^K(\phi, \gamma)$ is integrable since $h_F^K(\phi, \gamma) \leq C_{CN} r_K(\phi) r_K(\gamma)$ and $\iint_{-\pi}^{\pi} r_K(\phi) r_K(\gamma) d\phi d\gamma < \infty$ (finite area). By assumption A1, it follows that $r_K(\phi)$ converges uniformly to $r(\phi)$, for all ϕ . Hence, using bounded area, it can then be shown that $h_F^K(\cdot, \cdot)$ as defined in (15) converges uniformly to $h_F(\cdot, \cdot)$ as defined in (16). Also, the basis functions are square integrable. So, it follows that F_{ij}^K converges uniformly to F_{ij} as $K \rightarrow \infty$.

Hence, using Fubini's theorem

$$\begin{aligned}
 \lim_{K \rightarrow \infty} \sum_{i=1}^K F_{ii}^K &= \sum_{i=1}^{\infty} F_{ii} \\
 &= \sum_{i=1}^{\infty} \iint_{-\pi}^{\pi} h_F(\phi, \gamma) B_i(\phi) B_j(\gamma) d\phi d\gamma \\
 &= C_{CN} \int_{-\pi}^{\pi} h_F(\phi, \phi) d\phi, \quad \text{using (14)}
 \end{aligned} \tag{67}$$

$$\leq C_{\text{CN}} \int_{-\pi}^{\pi} r^2(\phi) d\phi \quad (68)$$

■

II. PROOF OF LEMMA 2 (UNCONSTRAINED CR BOUND FOR 2D SHAPE)

Suppose there exists an integrable function $h_G(\cdot, \cdot)$ that satisfies

$$\int_{-\pi}^{\pi} h_F(\phi, \psi) h_G(\psi, \gamma) d\psi = \delta(\phi, \gamma). \quad (69)$$

i.e. $h_G(\cdot, \cdot)$ is the inverse of $h_F(\cdot, \cdot)$ in the sense of operators. Recall that this exists only if $h_F(\cdot, \cdot)$ is positive definite.

If such a function $h_G(\cdot, \cdot)$ exists, then we will show that

$$G_{ij} := \iint_{-\pi}^{\pi} h_G(\phi, \gamma) B_i(\phi) B_j(\gamma) d\phi d\gamma \quad (70)$$

satisfies (20). Note that $h_G(\cdot, \cdot)$ is symmetric, since F_{ij} is symmetric. Now, again by Fubini's theorem,

$$\begin{aligned} & \sum_{l=1}^{\infty} F_{il} G_{lj} \\ &= \sum_{l=1}^{\infty} \iiint_{-\pi}^{\pi} h_F(\phi_1, \gamma_1) h_G(\phi_2, \gamma_2) B_i(\phi_1) B_l(\gamma_1) B_l(\phi_2) B_j(\gamma_2) d\phi_1 d\gamma_1 d\phi_2 d\gamma_2 \\ &= \iiint_{-\pi}^{\pi} h_G(\phi_2, \gamma_2) B_i(\phi_1) B_j(\gamma_2) \left[\sum_{l=1}^{\infty} \int_{-\pi}^{\pi} h_F(\phi_1, \gamma_1) B_l(\gamma_1) B_l(\phi_2) d\gamma_1 \right] d\phi_1 d\phi_2 d\gamma_2 \\ &= \iint_{-\pi}^{\pi} \left[\int_{-\pi}^{\pi} h_F(\phi_1, \phi_2) h_G(\phi_2, \gamma_2) d\phi_2 \right] B_i(\phi_1) B_j(\gamma_2) d\phi_1 d\gamma_2, \quad \text{from (14)} \\ &= \int_{-\pi}^{\pi} B_i(\phi_1) B_j(\phi_1) d\phi_1, \quad \text{using (69)} \\ &= \delta_{ij}, \quad \text{from (13)}. \end{aligned}$$

By symmetry, $\sum_{l=1}^{\infty} G_{il} F_{lj} = \delta_{ij}$. Hence, G_{ij} satisfies (20).

Using assumption A1, the covariance of $\hat{r}(\cdot)$ is given by

$$\text{cov}(\hat{r}(\phi), \hat{r}(\gamma)) = \lim_{K \rightarrow \infty} \sum_{i=1}^K \sum_{j=1}^K \text{cov}(\hat{\theta}_i, \hat{\theta}_j) B_i(\phi) B_j(\gamma).$$

By completeness of the given basis set, $\hat{r}(\cdot)$ lies in the linear span of the basis set. Therefore, using the CR bound for covariance of $\hat{\theta}_i$, we get

$$\text{cov}(\hat{r}(\phi), \hat{r}(\gamma)) - \lim_{K \rightarrow \infty} \sum_{i=1}^K \sum_{j=1}^K G_{ij} B_i(\phi) B_j(\gamma) \text{ is n.n.d.} \quad (71)$$

Note that, when G_{ij} satisfies (70), by Fubini

$$\begin{aligned} & \lim_{K \rightarrow \infty} \sum_{i=1}^K \sum_{j=1}^K G_{ij}^K B_i(\phi) B_j(\gamma) \\ &= \lim_{K \rightarrow \infty} \sum_{i=1}^K \sum_{j=1}^K \iint_{-\pi}^{\pi} h_G(\tilde{\phi}, \tilde{\gamma}) B_i(\tilde{\phi}) B_j(\tilde{\gamma}) B_i(\phi) B_j(\gamma) d\tilde{\phi} d\tilde{\gamma} \\ &= \sum_{i=1}^{\infty} \int_{-\pi}^{\pi} \left[\sum_{j=1}^{\infty} \int_{-\pi}^{\pi} h_G^K(\tilde{\phi}, \tilde{\gamma}) B_j(\tilde{\gamma}) B_j(\gamma) d\tilde{\gamma} \right] B_i(\tilde{\phi}) B_i(\phi) d\tilde{\phi} \\ &= \sum_{i=1}^{\infty} \int_{-\pi}^{\pi} h_G^K(\tilde{\phi}, \gamma) B_i(\tilde{\phi}) B_i(\phi) d\tilde{\phi}, \quad \text{from (14)} \\ &= h_G(\phi, \gamma), \quad \text{from (14)}. \end{aligned}$$

So, $\text{cov}(\hat{r}(\phi), \hat{r}(\gamma)) - h_G(\phi, \gamma)$ is n.n.d. ■

III. PROOF OF LEMMA 3 (UNIQUE 2D SHAPE SATISFYING AN ODE)

We would like to prove that the only star-shaped object that satisfies

$$\frac{r^2(\psi)}{\sqrt{r^2(\psi) + [r'(\psi)]^2}} = c, \quad \forall \psi \quad (72)$$

where c is a constant, is a circular disk.

Clearly, a circle (which has constant radius) satisfies (72). Here, we should recall that by ‘‘circle’’, we mean a circle defined around the center-of-description.

We observe that $c > 0$, for otherwise the shape is actually a point, which is a trivial solution. Also, we see that $r(\psi) > 0$ whenever $r'(\psi) \neq 0$. This tells us that shapes with boundary passing through its center-of-description are excluded, unless $r(\psi)$ and $r'(\psi)$ are both zero only at finitely many points.

Squaring both sides of (72), we get

$$\begin{aligned} r^4(\psi) &= c^2 r^2(\psi) + c^2 [r'(\psi)]^2 \\ [r'(\psi)]^2 &= r^2(\psi) \left[\frac{r^2(\psi)}{c^2} - 1 \right] \end{aligned} \quad (73)$$

Therefore, for $r'(\psi)$ to be real, we require,

$$r^2(\psi) \geq c^2 \quad (74)$$

$$\implies r(\psi) \geq c > 0, \forall \psi > 0 \text{ (since, } r(\psi) \geq 0) \quad (75)$$

Differentiating both sides of (73), we get

$$2r'(\psi)r''(\psi) = 2r(\psi) \left[\frac{2r^2(\psi)}{c^2} - 1 \right] r'(\psi) \quad (76)$$

Whenever $r'(\psi) \neq 0$, it is then true that

$$r''(\psi) = r(\psi) \left[\frac{2r^2(\psi)}{c^2} - 1 \right] \quad (77)$$

Recall from (74) that $\left[\frac{r^2(\psi)}{c^2} - 1 \right] \geq 0$ and from (75) that $r(\psi) > 0$. So we have

$$\left[\frac{2r^2(\psi)}{c^2} - 1 \right] > 0.$$

Note the strict inequality in the previous equation. So, it is true that whenever $r'(\psi) \neq 0$

$$r''(\psi) > 0. \quad (78)$$

Also note that when $r(\psi)$ increases, $r''(\psi)$ also increases and that when $r(\psi)$ decreases, $r''(\psi)$ also decreases.

Whenever $r'(\psi) = 0$, by differentiating (76), we get

$$2 [r''(\psi)]^2 + 2r'(\psi)r'''(\psi) = \frac{4}{c^2}r^3(\psi)r''(\psi) + \frac{12}{c^2}r^2(\psi) [r'(\psi)]^2 - 2r(\psi)r''(\psi) - 2 [r'(\psi)]^2.$$

Since $r'(\psi) = 0$ and $r'''(\psi)$ is finite we get

$$[r''(\psi)]^2 = \frac{2r^3(\psi)}{c^2}r''(\psi) - r(\psi)r''(\psi).$$

Therefore, when $r'(\psi) = 0$ and $r''(\psi) \neq 0$, we get

$$\begin{aligned} r''(\psi) &= \frac{2r^3(\psi)}{c^2} - r(\psi) \\ &= r(\psi) \left[\frac{2r^2(\psi)}{c^2} - 1 \right] \\ &> 0 \text{ (from equations (74) and (75)).} \end{aligned}$$

So, it is true that whenever $r'(\psi) = 0$

$$r''(\psi) \geq 0. \quad (79)$$

So, from equations (78) and (79), it is true that

$$r''(\psi) \geq 0 \text{ (with strict inequality whenever } r'(\psi) \neq 0\text{)}. \quad (80)$$

Let ξ and ω be angles such that $\omega - \pi \leq \xi \leq \omega + \pi$. Then

$$\int_{\psi=\omega-\pi}^{\xi} r''(\psi) d\psi = r'(\xi) - r'(\omega - \pi).$$

Again,

$$\begin{aligned} \int_{\xi=\omega-\pi}^{\omega+\pi} \int_{\psi=\omega-\pi}^{\xi} r''(\psi) d\psi d\xi &= \int_{\xi=\omega-\pi}^{\omega+\pi} r'(\xi) d\xi - \int_{\xi=\omega-\pi}^{\omega+\pi} r'(\omega - \pi) d\xi \\ &= \underbrace{r(\omega + \pi) - r(\omega - \pi)}_{= 0} - 2\pi r'(\omega - \pi) \\ &= 0 \text{ (since the boundary is a closed curve)} \end{aligned}$$

Thus,

$$\forall \omega \in \mathbb{R} : \int_{\xi=\omega-\pi}^{\omega+\pi} \int_{\psi=\omega-\pi}^{\xi} r''(\psi) d\psi d\xi = -2\pi r'(\omega - \pi). \quad (81)$$

Note that from (80), we get

$$\forall \omega \in \mathbb{R} : \int_{\xi=\omega-\pi}^{\omega+\pi} \int_{\psi=\omega-\pi}^{\xi} r''(\psi) d\psi d\xi \geq 0. \quad (82)$$

However, since ω is arbitrary and since we ignore the ‘‘point object’’, which is a trivial solution, and eliminate the circle for which $\forall \omega : r'(\omega - \pi) = 0$, there exists atleast one ω for which $r'(\omega - \pi) > 0$. So, we get from (81) that

$$\exists \omega \in \mathbb{R} : \int_{\xi=\omega-\pi}^{\omega+\pi} \int_{\psi=\omega-\pi}^{\xi} r''(\psi) d\psi d\xi < 0.$$

This contradicts (82). Thus, we have proven that the only smooth star-shaped object that satisfies (72) is the circle. ■

IV. PROOF OF LEMMA 4 (FISHER INFORMATION FOR 3D SHAPE)

We will follow a procedure similar to the 2D case as in [33, pp. 139–142]. Define $I_{\theta}^s(x, y, z) = (I_{\theta} \star \star \star H)(x, y, z)$.

Then the log-likelihood is given by

$$\ln f(Y_M, \theta) = C + \left(\frac{-1}{2\sigma_n^2} \right) \cdot \iiint_{R_f} [Y_M(x, y, z) - I_{\theta}^s(x, y, z)]^2 dx dy dz \quad (83)$$

where C is independent of θ and R_f is the field of view. Thus,

$$\begin{aligned}\nabla_{\theta} \ln f(Y_M, \theta) &= \left(\frac{-1}{\sigma_n^2}\right) \cdot \iiint_{R_f} [Y_M(x, y, z) - I_{\theta}^s(x, y, z)] \nabla_{\theta} I_{\theta}^s dx dy dz \\ \nabla_{\theta}^2 \ln f(Y_M, \theta) &= \\ &\left(\frac{1}{\sigma_n^2}\right) \cdot \iiint_{R_f} \left[\underbrace{(Y_M(x, y, z) - I_{\theta}^s(x, y, z))}_{= n(x, y, z)} \nabla_{\theta}^2 I_{\theta}^s - \nabla_{\theta} I_{\theta}^s \cdot \nabla_{\theta}^T I_{\theta}^s \right] dx dy dz\end{aligned}$$

Taking expectation of negative Hessian,

$$E[-\nabla_{\theta}^2 \ln f(Y_M, \theta)] = \left(\frac{1}{\sigma_n^2}\right) \cdot \iiint_{R_f} \nabla_{\theta} I_{\theta}^s \cdot \nabla_{\theta}^T I_{\theta}^s dx dy dz \quad (84)$$

Recall

$$\begin{aligned}I_{\theta}(x, y, z) &= C_{ROI} \cdot I_{R_{\theta}}(x, y, z) + C_{BG} \cdot (I_{R_f}(x, y, z) - I_{R_{\theta}}(x, y, z)) \\ &= (C_{ROI} - C_{BG}) \cdot I_{R_{\theta}}(x, y, z) + C_{BG} \cdot I_{R_f}(x, y, z) \\ \Rightarrow \nabla_{\theta} I_{\theta}^s(x, y, z) &= (C_{ROI} - C_{BG}) \cdot \nabla_{\theta} (I_{R_{\theta}} * * * H)(x, y, z).\end{aligned} \quad (85)$$

Let $C_s := \frac{C_{ROI} - C_{BG}}{(2\pi)^{3/2} \sigma_s^3}$. Writing $I_{\theta}^s(x, y, z)$ explicitly, we get

$$I_{\theta}^s(x, y, z) = C_s \cdot \iiint_{R_{\theta}} \exp\left[\frac{(x - \tau_1)^2 + (y - \tau_2)^2 + (z - \tau_3)^2}{-2\sigma_s^2}\right] d\tau_1 d\tau_2 d\tau_3 \quad (86)$$

Consider the cartesian coordinate (x, y, z) to spherical coordinate (r, α, β) transformation defined by (see Figure 8):

$$x = r \cos \alpha \cos \beta$$

$$y = r \cos \alpha \sin \beta$$

$$z = r \sin \alpha$$

where α, β are the parameters for elevation and azimuth angles respectively.

The Jacobian for this transformation is given by $r^2 \cos \alpha$.

Therefore,

$$\begin{aligned}I_{\theta}^s(x, y, z) &= C_s \cdot \int_{\alpha=-\frac{\pi}{2}}^{\frac{\pi}{2}} \int_{\beta=-\pi}^{\pi} \int_{\gamma=0}^{r_{\theta}(\alpha, \beta)} \\ \exp\left[\frac{(x - \gamma \cos \alpha \cos \beta)^2 + (y - \gamma \cos \alpha \sin \beta)^2 + (z - \gamma \sin \alpha)^2}{-2\sigma_s^2}\right] &\gamma^2 \cos \alpha d\gamma d\alpha d\beta.\end{aligned} \quad (87)$$

By applying Leibnitz's rule for differentiation of integral, we obtain

$$\nabla_{\theta} \mathbf{I}_{\theta}^s(x, y, z) = C_s \cdot \int_{\alpha=-\frac{\pi}{2}}^{\frac{\pi}{2}} \int_{\beta=-\pi}^{\pi} \exp \left[\frac{(x - r_{\theta}(\alpha, \beta) \cos \alpha \cos \beta)^2 + (y - r_{\theta}(\alpha, \beta) \cos \alpha \sin \beta)^2 + (z - r_{\theta}(\alpha, \beta) \sin \alpha)^2}{-2\sigma_s^2} \right] \cdot r_{\theta}^2(\alpha, \beta) \cos \alpha (\nabla_{\theta} r_{\theta}(\alpha, \beta)) d\alpha d\beta.$$

Let $f(\theta, x, y, z, \alpha, \beta) :=$

$$\exp \left[\frac{(x - r_{\theta}(\alpha, \beta) \cos \alpha \cos \beta)^2 + (y - r_{\theta}(\alpha, \beta) \cos \alpha \sin \beta)^2 + (z - r_{\theta}(\alpha, \beta) \sin \alpha)^2}{-2\sigma_s^2} \right]$$

and $g(\theta, \alpha_1, \alpha_2, \beta_1, \beta_2) :=$

$$r_{\theta}^2(\alpha_1, \beta_1) r_{\theta}^2(\alpha_2, \beta_2) (\nabla_{\theta} r_{\theta}(\alpha_1, \beta_1)) (\nabla_{\theta}^T r_{\theta}(\alpha_2, \beta_2)) \cos \alpha_1 \cos \alpha_2.$$

Then the Fisher information is given by

$$\mathbf{F}_{\theta} = \frac{C_s^2}{\sigma_n^2} \cdot \iiint_{R_f} \int_{\alpha_1=-\frac{\pi}{2}}^{\frac{\pi}{2}} \int_{\beta_1=-\pi}^{\pi} \int_{\alpha_2=-\frac{\pi}{2}}^{\frac{\pi}{2}} \int_{\beta_2=-\pi}^{\pi} f(\theta, x, y, z, \alpha_1, \beta_1) f(\theta, x, y, z, \alpha_2, \beta_2) g(\theta, \alpha_1, \alpha_2, \beta_1, \beta_2) d\alpha_1 d\beta_1 d\alpha_2 d\beta_2 dx dy dz.$$

Note that

(88)

$$\begin{aligned} & (x - r_{\theta}(\alpha, \beta) \cos \alpha \cos \beta)^2 + (y - r_{\theta}(\alpha, \beta) \cos \alpha \sin \beta)^2 + (z - r_{\theta}(\alpha, \beta) \sin \alpha)^2 \\ &= x^2 - 2xr_{\theta}(\alpha, \beta) \cos \alpha \cos \beta + r_{\theta}^2(\alpha, \beta) \cos^2 \alpha \cos^2 \beta \\ & \quad + y^2 - 2yr_{\theta}(\alpha, \beta) \cos \alpha \sin \beta + r_{\theta}^2(\alpha, \beta) \cos^2 \alpha \sin^2 \beta \\ & \quad + z^2 - 2zr_{\theta}(\alpha, \beta) \sin \alpha + r_{\theta}^2(\alpha, \beta) \sin^2 \alpha \\ &= x^2 + y^2 + z^2 + r_{\theta}^2(\alpha, \beta) - 2r_{\theta}(\alpha, \beta) (x \cos \alpha \cos \beta + y \cos \alpha \sin \beta + z \sin \alpha). \end{aligned}$$

Let us denote the numerator of the negative exponent in the product $f(\theta, x, y, z, \alpha_1, \beta_1) \cdot f(\theta, x, y, z, \alpha_2, \beta_2)$ by \mathcal{N} .

Then \mathcal{N} can be written as

$$\begin{aligned} \mathcal{N} &= 2 [x^2 - x (r_{\theta}(\alpha_1, \beta_1) \cos \alpha_1 \cos \beta_1 + r_{\theta}(\alpha_2, \beta_2) \cos \alpha_2 \cos \beta_2)] \\ & \quad + 2 [y^2 - y (r_{\theta}(\alpha_1, \beta_1) \cos \alpha_1 \sin \beta_1 + r_{\theta}(\alpha_2, \beta_2) \cos \alpha_2 \sin \beta_2)] \\ & \quad + 2 [z^2 - z (r_{\theta}(\alpha_1, \beta_1) \sin \alpha_1 + r_{\theta}(\alpha_2, \beta_2) \sin \alpha_2)] \\ & \quad + r_{\theta}^2(\alpha_1, \beta_1) + r_{\theta}^2(\alpha_2, \beta_2). \end{aligned}$$

Let us now define

$$\begin{aligned} a &= r_{\theta}(\alpha_1, \beta_1) \cos \alpha_1 \cos \beta_1 + r_{\theta}(\alpha_2, \beta_2) \cos \alpha_2 \cos \beta_2 \\ b &= r_{\theta}(\alpha_1, \beta_1) \cos \alpha_1 \sin \beta_1 + r_{\theta}(\alpha_2, \beta_2) \cos \alpha_2 \sin \beta_2 \\ c &= r_{\theta}(\alpha_1, \beta_1) \sin \alpha_1 + r_{\theta}(\alpha_2, \beta_2) \sin \alpha_2. \end{aligned}$$

Using this, we can write \mathcal{N} as

$$\mathcal{N} = 2(x^2 - ax) + 2(y^2 - by) + 2(z^2 - cz) + r_{\theta}^2(\alpha_1, \beta_1) + r_{\theta}^2(\alpha_2, \beta_2). \quad (89)$$

Completing the squares,

$$\begin{aligned} \mathcal{N} &= 2 \left[\left(x - \frac{a}{2}\right)^2 + \left(y - \frac{b}{2}\right)^2 + \left(z - \frac{c}{2}\right)^2 \right] - \frac{1}{2}(a^2 + b^2 + c^2) \\ &\quad + r_{\theta}^2(\alpha_1, \beta_1) + r_{\theta}^2(\alpha_2, \beta_2) \end{aligned} \quad (90)$$

Define

$$\begin{aligned} D &:= r_{\theta}^2(\alpha_1, \beta_1) + r_{\theta}^2(\alpha_2, \beta_2) - \frac{1}{2}(a^2 + b^2 + c^2) \\ \text{and } A_g &:= \left[\left(x - \frac{a}{2}\right)^2 + \left(y - \frac{b}{2}\right)^2 + \left(z - \frac{c}{2}\right)^2 \right]. \end{aligned}$$

Then, $\mathcal{N} = 2A_g + D$. We make the following approximation:

$$\iiint_{R_f} \exp\left(\frac{A_g}{-\sigma_s^2}\right) dx dy dz \approx (2\pi)^{3/2} \cdot \left(\frac{\sigma_s^2}{2}\right)^{3/2} = (\pi\sigma_s^2)^{3/2}.$$

From the definitions of D and A_g , we can write the Fisher information of (88) as

$$\begin{aligned} \mathbf{F}_{\theta} &= \frac{C_s^2}{\sigma_n^2} \cdot \int_{\alpha_1=-\frac{\pi}{2}}^{\frac{\pi}{2}} \int_{\beta_1=-\pi}^{\pi} \int_{\alpha_2=-\frac{\pi}{2}}^{\frac{\pi}{2}} \int_{\beta_2=-\pi}^{\pi} g(\theta, \alpha_1, \alpha_2, \beta_1, \beta_2) \cdot \exp\left(\frac{D}{-2\sigma_s^2}\right) \\ &\quad \iiint_{R_f} \exp\left(\frac{A_g}{-\sigma_s^2}\right) dx dy dz d\alpha_1 d\beta_1 d\alpha_2 d\beta_2 \end{aligned} \quad (91)$$

$$\begin{aligned} &\approx \frac{C_s^2 (\pi\sigma_s^2)^{3/2}}{\sigma_n^2} \cdot \int_{\alpha_1=-\frac{\pi}{2}}^{\frac{\pi}{2}} \int_{\beta_1=-\pi}^{\pi} \int_{\alpha_2=-\frac{\pi}{2}}^{\frac{\pi}{2}} \int_{\beta_2=-\pi}^{\pi} g(\theta, \alpha_1, \alpha_2, \beta_1, \beta_2) \\ &\quad \cdot \exp\left(\frac{D}{-2\sigma_s^2}\right) d\alpha_1 d\beta_1 d\alpha_2 d\beta_2. \end{aligned} \quad (92)$$

Now,

$$\begin{aligned}
a^2 &= r_{\theta}^2(\alpha_1, \beta_1) \cos^2 \alpha_1 \cos^2 \beta_1 + r_{\theta}^2(\alpha_2, \beta_2) \cos^2 \alpha_2 \cos^2 \beta_2 \\
&\quad + 2r_{\theta}(\alpha_1, \beta_1)r_{\theta}(\alpha_2, \beta_2) \cos \alpha_1 \cos \beta_1 \cos \alpha_2 \cos \beta_2 \\
b^2 &= r_{\theta}^2(\alpha_1, \beta_1) \cos^2 \alpha_1 \sin^2 \beta_1 + r_{\theta}^2(\alpha_2, \beta_2) \cos^2 \alpha_2 \sin^2 \beta_2 \\
&\quad + 2r_{\theta}(\alpha_1, \beta_1)r_{\theta}(\alpha_2, \beta_2) \cos \alpha_1 \sin \beta_1 \cos \alpha_2 \sin \beta_2 \\
c^2 &= r_{\theta}^2(\alpha_1, \beta_1) \sin^2 \alpha_1 + r_{\theta}^2(\alpha_2, \beta_2) \sin^2 \alpha_2 + 2r_{\theta}(\alpha_1, \beta_1)r_{\theta}(\alpha_2, \beta_2) \sin \alpha_1 \sin \alpha_2.
\end{aligned}$$

Therefore,

$$\begin{aligned}
a^2 + b^2 + c^2 &= r_{\theta}^2(\alpha_1, \beta_1) + r_{\theta}^2(\alpha_2, \beta_2) \\
&\quad + 2r_{\theta}(\alpha_1, \beta_1)r_{\theta}(\alpha_2, \beta_2) [\sin \alpha_1 \sin \alpha_2 + \cos \alpha_1 \cos \alpha_2 \cos(\beta_1 - \beta_2)].
\end{aligned}$$

Therefore,

$$\begin{aligned}
D &= \frac{1}{2} \{ r_{\theta}^2(\alpha_1, \beta_1) + r_{\theta}^2(\alpha_2, \beta_2) \\
&\quad - 2r_{\theta}(\alpha_1, \beta_1)r_{\theta}(\alpha_2, \beta_2) [\sin \alpha_1 \sin \alpha_2 + \cos \alpha_1 \cos \alpha_2 \cos(\beta_1 - \beta_2)] \}.
\end{aligned}$$

Consider two points (r_1, α_1, β_1) and (r_2, α_2, β_2) in a three dimensional space. The square of the Euclidean distance between them is given by

$$\begin{aligned}
\|\vec{r}(\alpha_1, \beta_1) - \vec{r}(\alpha_2, \beta_2)\|^2 &= (r_1 \cos \alpha_1 \cos \beta_1 - r_2 \cos \alpha_2 \cos \beta_2)^2 \\
&\quad + (r_1 \cos \alpha_1 \sin \beta_1 - r_2 \cos \alpha_2 \sin \beta_2)^2 + (r_1 \sin \alpha_1 - r_2 \sin \alpha_2)^2 \\
&= r_1^2 \cos^2 \alpha_1 \cos^2 \beta_1 + r_2^2 \cos^2 \alpha_2 \cos^2 \beta_2 - 2r_1 r_2 \cos \alpha_1 \cos \beta_1 \cos \alpha_2 \cos \beta_2 \\
&\quad + r_1^2 \cos^2 \alpha_1 \sin^2 \beta_1 + r_2^2 \cos^2 \alpha_2 \sin^2 \beta_2 - 2r_1 r_2 \cos \alpha_1 \sin \beta_1 \cos \alpha_2 \sin \beta_2 \\
&\quad + r_1^2 \sin^2 \alpha_1 + r_2^2 \sin^2 \alpha_2 - 2r_1 r_2 \sin \alpha_1 \sin \alpha_2 \\
&= r_1^2 + r_2^2 - 2r_1 r_2 (\cos \alpha_1 \cos \alpha_2 \cos(\beta_1 - \beta_2) + \sin \alpha_1 \sin \alpha_2).
\end{aligned}$$

Using this formula for Euclidean distance, we observe that

$$D = \|r_{\theta}(\alpha_1, \beta_1) - r_{\theta}(\alpha_2, \beta_2)\|^2/2.$$

So, we can write the Fisher information in (92) as²

$$[\mathbf{F}_\theta]_{i,j} = C_{CN} \cdot \int_{\alpha_1=-\frac{\pi}{2}}^{\frac{\pi}{2}} \int_{\beta_1=-\pi}^{\pi} \int_{\alpha_2=-\frac{\pi}{2}}^{\frac{\pi}{2}} \int_{\beta_2=-\pi}^{\pi} \exp\left(\frac{\|r_\theta(\alpha_1, \beta_1) - r_\theta(\alpha_2, \beta_2)\|^2}{-4\sigma_s^2}\right) r_\theta^2(\alpha_1, \beta_1) r_\theta^2(\alpha_2, \beta_2) \cdot B_i(\alpha_1, \beta_1); B_j(\alpha_2, \beta_2) \cos \alpha_1 \cos \alpha_2 d\alpha_1 d\beta_1 d\alpha_2 d\beta_2 \quad (93)$$

where $C_{CN} := \frac{C_s^2(\pi\sigma_s^2)^{3/2}}{\sigma_n^2}$ and $\nabla_\theta r_\theta(\alpha, \beta) = B_i(\alpha, \beta)$. Here, $B_i(\alpha, \beta)$ is value of the i -th basis at elevation and azimuth angles (α, β) . ■

V. PROOF OF LEMMA 5 (ASYMPTOTIC FISHER INFORMATION FOR 3D SHAPE)

We will reduce the complexity of the \mathbf{F}_θ in (43) by reducing the number of integrals to 2. In order to achieve this, we will collect all terms that involve α_1 and β_1 . Define the vector

$$\mathbf{A}(\alpha_2, \beta_2) := \int_{\alpha_1=-\frac{\pi}{2}}^{\frac{\pi}{2}} \int_{\beta_1=-\pi}^{\pi} \exp\left(\frac{\|\vec{r}_\theta(\alpha_1, \beta_1) - \vec{r}_\theta(\alpha_2, \beta_2)\|^2}{-4\sigma_s^2}\right) \cdot r_\theta^2(\alpha_1, \beta_1) \mathbf{B}(\alpha_1, \beta_1) \cos \alpha_1 d\alpha_1 d\beta_1$$

so that

$$\mathbf{F}_\theta = C_{CN} \cdot \int_{\alpha_2=-\frac{\pi}{2}}^{\frac{\pi}{2}} \int_{\beta_2=-\pi}^{\pi} \mathbf{A}(\alpha_2, \beta_2) r_\theta^2(\alpha_2, \beta_2) \mathbf{B}^T(\alpha_2, \beta_2) \cos \alpha_2 d\alpha_2 d\beta_2 \quad (94)$$

Using Taylor's series expansion with remainder for the vector $\vec{r}_\theta(\alpha_1, \beta_1)$,

$$\begin{aligned} \vec{r}_\theta(\alpha_1, \beta_1) &= \vec{r}_\theta(\alpha_2, \beta_2) + \vec{r}_\theta^{10}(\alpha_2, \beta_2)(\alpha_1 - \alpha_2) + \vec{r}_\theta^{01}(\alpha_2, \beta_2)(\beta_1 - \beta_2) \\ &+ \frac{1}{2} \{ \vec{r}_\theta^{20}(\alpha_1^*, \beta_1^*)(\alpha_1 - \alpha_2)^2 + 2\vec{r}_\theta^{11}(\alpha_2^*, \beta_2^*)(\alpha_1 - \alpha_2)(\beta_1 - \beta_2) + \vec{r}_\theta^{02}(\alpha_2^*, \beta_2^*)(\beta_1 - \beta_2)^2 \} \end{aligned} \quad (95)$$

where α_2^* is a point between α_1 and α_2 on the line segment connecting them; similarly, β_2^* is a point between β_1 and β_2 on the line segment connecting them. Thus,

$$\begin{aligned} \|\vec{r}_\theta(\alpha_1, \beta_1) - \vec{r}_\theta(\alpha_2, \beta_2)\|^2 &= \|\vec{r}_\theta^{10}(\alpha_2, \beta_2)\|^2 (\alpha_1 - \alpha_2)^2 + \|\vec{r}_\theta^{01}(\alpha_2, \beta_2)\|^2 (\beta_1 - \beta_2)^2 \\ &+ 2 \langle \vec{r}_\theta^{10}(\alpha_2, \beta_2), \vec{r}_\theta^{01}(\alpha_2, \beta_2) \rangle (\alpha_1 - \alpha_2)(\beta_1 - \beta_2) + Q_\theta(\alpha_1, \beta_1, \alpha_2, \beta_2) \end{aligned} \quad (96)$$

where $Q_\theta(\alpha_1, \beta_1, \alpha_2, \beta_2)$ consists of higher order terms of order less than $(\alpha_1 - \alpha_2)^2 + (\beta_1 - \beta_2)^2$.

²For clarity, we ignore the approximation symbol and use equality.

Recall definitions of $\sigma_1(\alpha_2, \beta_2)$, $\sigma_2(\alpha_2, \beta_2)$ and $\rho_{\theta}(\alpha_2, \beta_2)$ from equations (46), (47) and (48). Consider the Gaussian kernel $G_{\theta, \alpha_2, \beta_2}(\alpha_1, \beta_1)$ with mean α_2, β_2 and spread factors $\sigma_1(\alpha_2, \beta_2), \sigma_2(\alpha_2, \beta_2)$ respectively and coefficient $\rho_{\theta}(\alpha_2, \beta_2)$:

$$G_{\theta, \alpha_2, \beta_2}(\alpha_1, \beta_1) := \frac{1}{2\pi \sigma_1(\alpha_2, \beta_2), \sigma_2(\alpha_2, \beta_2) \sqrt{1 - \rho_{\theta}^2(\alpha_2, \beta_2)}} \cdot \exp \left\{ \frac{-1}{2\sqrt{1 - \rho_{\theta}^2(\alpha_2, \beta_2)}} \left[\left(\frac{\alpha_1 - \alpha_2}{\sigma_1(\alpha_2, \beta_2)} \right)^2 + 2\rho_{\theta}(\alpha_2, \beta_2) \frac{(\alpha_1 - \alpha_2)(\beta_1 - \beta_2)}{\sigma_1(\alpha_2, \beta_2)\sigma_2(\alpha_2, \beta_2)} + \left(\frac{\beta_1 - \beta_2}{\sigma_2(\alpha_2, \beta_2)} \right)^2 \right] \right\} \quad (97)$$

Substituting for $\sigma_1(\alpha_2, \beta_2), \sigma_2(\alpha_2, \beta_2)$ and $\rho_{\theta}(\alpha_2, \beta_2)$,

$$G_{\theta, \alpha_2, \beta_2}(\alpha_1, \beta_1) := \frac{\sqrt{\|\vec{r}_{\theta}^{10}(\alpha_2, \beta_2)\|^2 \|\vec{r}_{\theta}^{01}(\alpha_2, \beta_2)\|^2 - \langle \vec{r}_{\theta}^{10}(\alpha_2, \beta_2), \vec{r}_{\theta}^{01}(\alpha_2, \beta_2) \rangle^2}}{4\pi \sigma_s^2} \times \exp \left\{ \frac{-1}{4\sigma_s^2} \left[\|\vec{r}_{\theta}^{10}(\alpha_2, \beta_2)\|^2 (\alpha_1 - \alpha_2)^2 + 2 \langle \vec{r}_{\theta}^{10}(\alpha_2, \beta_2), \vec{r}_{\theta}^{01}(\alpha_2, \beta_2) \rangle (\alpha_1 - \alpha_2)(\beta_1 - \beta_2) + \|\vec{r}_{\theta}^{01}(\alpha_2, \beta_2)\|^2 (\beta_1 - \beta_2)^2 \right] \right\} \quad (98)$$

Define the vector

$$\mathbf{g}(\alpha_1, \beta_1) := \exp \{ Q_{\theta}(\alpha_1, \beta_1, \alpha_2, \beta_2) \} r_{\theta}^2(\alpha_1, \beta_1) \mathbf{B}(\alpha_1, \beta_1) \cos \alpha_1. \quad (99)$$

Therefore

$$\mathbf{A}(\alpha_2, \beta_2) = \frac{4\pi \sigma_s^2}{\sqrt{\|\vec{r}_{\theta}^{10}(\alpha_2, \beta_2)\|^2 \|\vec{r}_{\theta}^{01}(\alpha_2, \beta_2)\|^2 - \langle \vec{r}_{\theta}^{10}(\alpha_2, \beta_2), \vec{r}_{\theta}^{01}(\alpha_2, \beta_2) \rangle^2}} \times \int_{\alpha_1 = -\frac{\pi}{2}}^{\frac{\pi}{2}} \int_{\beta_1 = -\pi}^{\pi} g(\alpha_1, \beta_1) G_{\theta, \alpha_2, \beta_2}(\alpha_1, \beta_1) d\alpha_1 d\beta_1 \quad (100)$$

Finally we show that to order $o(\sigma_m)$, where $\sigma_m = \max_{\alpha, \beta} \frac{\sigma_1(\alpha, \beta) + \sigma_2(\alpha, \beta)}{2}$, the double integral evaluates to $\mathbf{g}(\alpha_2, \beta_2)$.

This occurs since for small σ_m and fixed α_1, β_1 the width of the Gaussian kernel in α_2, β_2 is considerably narrower than the width of $g(\alpha_2, \beta_2)$.

$$\mathbf{A}(\alpha_2, \beta_2) = \frac{4\pi \sigma_s^2 r_{\theta}^2(\alpha_2, \beta_2) \mathbf{B}(\alpha_2, \beta_2) \cos \alpha_2}{\sqrt{\|\vec{r}_{\theta}^{10}(\alpha_2, \beta_2)\|^2 \|\vec{r}_{\theta}^{01}(\alpha_2, \beta_2)\|^2 - \langle \vec{r}_{\theta}^{10}(\alpha_2, \beta_2), \vec{r}_{\theta}^{01}(\alpha_2, \beta_2) \rangle^2}} + o(\sigma_m).. \quad (101)$$

Here we used the fact that $\lim_{\xi \rightarrow 0} \xi \exp(-c\xi) = 0$ for $c > 0$. Defining

$$h_{\theta}(\alpha_2, \beta_2) := \frac{r_{\theta}^4(\alpha_2, \beta_2)}{\sqrt{\|\vec{r}_{\theta}^{10}(\alpha_2, \beta_2)\|^2 \|\vec{r}_{\theta}^{01}(\alpha_2, \beta_2)\|^2 - \langle \vec{r}_{\theta}^{10}(\alpha_2, \beta_2), \vec{r}_{\theta}^{01}(\alpha_2, \beta_2) \rangle^2}} \quad (102)$$

we obtain

$$\mathbf{F}_\theta = 4\pi C_{CN} \sigma_s^2 \int_{\alpha_2=-\frac{\pi}{2}}^{\frac{\pi}{2}} \int_{\beta_2=-\pi}^{\pi} h_\theta(\alpha_2, \beta_2) \mathbf{B}(\alpha_2, \beta_2) \mathbf{B}^T(\alpha_2, \beta_2) \cos^2 \alpha_2 d\alpha_2 d\beta_2 + o(\sigma_m). \quad (103)$$

■

REFERENCES

- [1] V. Berzins, "Accuracy of Laplacian edge detectors," *Computer Vision, Graphics, and Image Processing*, vol. 27, pp. 1955–2010, 1984.
- [2] F. L. Bookstein, "Principal warps: Thin-plate splines and the decomposition of deformations," *IEEE Transactions on Pattern Analysis and Machine Intelligence*, vol. 11, no. 6, pp. 567–585, June 1989.
- [3] M. Bret, *Image Synthesis*, Kluwer Academic Publishers, 1992.
- [4] J. Canny, "A computational approach to edge detection," *IEEE Transaction on Pattern Analysis and Machine Intelligence*, vol. COM-26, pp. 297–307, 1977.
- [5] S. Erturk and T. J. Dennis, "3d model representation using spherical harmonics," *Electronics Letters*, vol. 33, pp. 951–952, 1997.
- [6] M. A. Fischler and R. A. Elschlager, "The representation and matching of pictorial structures," *IEEE Transactions on Computers*, vol. C-22, no. 1, pp. 67–92, January 1973.
- [7] R. A. Fisher, "Theory of statistical estimation," *Proc. Cambridge Philosophical Society*, vol. 22, pp. 700–725, 1925.
- [8] E. Gose, R. Johnsonbaugh, and S. Jost, *Pattern recognition and image analysis*, Prentice Hall, 1996.
- [9] H. W. Guggenheimer, *Differential Geometry*, Dover, New York, NY, 1977.
- [10] P. Haigron, G. Lefaix, X. Riot, and R. Collorec, "Application of spherical harmonics to the modeling of anatomical shapes," *Journ. of Computing and Inform. Tech.*, vol. 6, pp. 449–461, 1998.
- [11] A. O. Hero, R. Piramuthu, S. R. Titus, and J. A. Fessler, "Minimax emission computed tomography using high resolution anatomical side information and B-spline models," *Special Issue of IEEE Transactions on Information Theory on Statistical Multiscale Analysis*, to appear in April 1999.
- [12] P. V. C. Hough, *A method and means for recognizing complex patterns*, U.S. Patent 3,069,654, 1962.
- [13] I. A. Ibragimov and R. Z. Has'minskii, *Statistical estimation: Asymptotic theory*, Springer-Verlag, New York, 1981.
- [14] J. Illingworth and J. Kittler, "The adaptive Hough transform," *Computer Vision, Graphics, and Image Processing*, vol. 44, no. 1, pp. 87–116, 1988.
- [15] A. K. Jain, Y. Zhong, and J. M. P. Dubuisson, "Deformable template models: a review," *Signal Processing*, vol. 71, no. 2, pp. 109–129, December 1998.
- [16] M. Kass, A. Witkin, and D. Terzopoulos, "Snakes: Active contour models," *International Journal of Computerr Vision*, vol. 1, no. 4, pp. 321–331, 1987.
- [17] A. Kelemen, G. Szekely, and G. Gerig, "Three dimensional model-based segmentation of brain MRI," in *Workshop on Biomedical Image Analysis: IEEE Computer Society*, Los Alamitos, CA, 1998.
- [18] R. Kirsch, "Computer determination of the constituent structure," *Computers and biomedical research*, vol. 4, pp. 315–328, 1971.
- [19] U. Lee, S. Y. Chung, and R. H. Park, "A comparative performance study of several global thresholding techniques for segmentation," *Computer Vision, Graphics, and Image Processing*, vol. 52, pp. 171–190, 1990.
- [20] R. Malladi and J. A. Sethian, "Level set and fast marching methods in image processing and computer vision," *Proceedings of ICIP*, vol. 1, pp. 489–492, 1996.
- [21] R. Malladi, J. A. Sethian, and B. C. Vemuri, "Shape modeling with front propagation: A level set approach," *IEEE Transactions on Pattern Analysis and Machine Intelligence*, vol. 17, no. 2, pp. 158–174, 1995.
- [22] D. Marr and E. C. Hildreth, "Theory of edge detection," *Proceedings of the Royal Society of London*, vol. 207, pp. 187–217, 1980.
- [23] A. Matheny, "The use of three and four dimensional surface harmonics for rigid and non-rigid shape recovery and representation," *IEEE Trans. on Pattern Anal. and Machine Intell.*, vol. PAMI-17, no. 10, pp. 967–981, Oct 1995.
- [24] T. McInerney and D. Terzopoulos, "Topologically adaptable snakes," *Proceedings of IEEE International Conference on Computer Vision*, pp. 840–845, 1995.
- [25] S. Osher and J. A. Sethian, "Fronts propagating with curvature-dependent speed: Algorithms based on Hamilton-Jacobi formulations," *Journal of Computational Physics*, vol. 79, pp. 12–49, 1988.
- [26] J. C. Russ, *The image processing handbook*, CRC Press, 1999.
- [27] J. A. Sethian, "Fast marching level set methods for three-dimensional photolithography development," *Proceedings of the SPIE*, vol. 2726, pp. 262–272, 1996.
- [28] I. Sobel, *Camera models and machine perception*, AIM-21, Stanford Artificial Intelligence Lab, Palo Alto, 1970.
- [29] M. Sonka, V. Hlavac, and R. Boyle, *Image processing, analysis and machine vision*, Chapman and Hall Computing, 1993.
- [30] S. K. Stein, *Calculus and analytic geometry*, Mc-Graw-Hill Book Company, 1982.
- [31] J. Strackee and N. J. D. Nagelkerke, "On closing the Fourier descriptor presentation," *IEEE Transactions on Pattern Analysis and Machine Intelligence*, vol. 5, no. 6, pp. 660–661, 1983.
- [32] G. B. Thomas and R. L. Finney, *Calculus and Analytic Geometry*, Addison-Wesley, Fifth Edition, 1979.
- [33] S. R. Titus, *Improved penalized likelihood reconstruction of anatomically correlated emission computed tomography data*, PhD thesis, The University of Michigan, Ann Arbor, December 1996.
- [34] H. L. Van-Trees, *Detection, Estimation, and Modulation Theory: Part I*, Wiley, New York, 1968.
- [35] D. von Seggern, *Curves and Surfaces*, CRC Press, Boca Raton, FL, 1993.
- [36] T. P. Wallace and P. A. Wintz, "An efficient three dimensional aircraft recognition algorithm using normalized Fourier descriptors," *Computer Graphics and Image Processing*, vol. 13, pp. 99–126, 1980.
- [37] J.-Y. Wang and F. S. Cohen, "3d object recognition and shape estimation from image contours using b-splines, shape invariant matching, and neural network," *IEEE Transactions on Pattern Analysis and Machine Intelligence*, vol. 16, no. 1, , January 1994.
- [38] A. Yezzi, S. Kichenassamy, A. Kumar, P. Olver, and A. Tannenbaum, "A geometric snake model for segmentation of medical imagery," *IEEE Transactions on Medical Imaging*, vol. 16, no. 2, pp. 199–209, Apr. 1997.
- [39] Y. Zheng and P. Doerschuk, "Explicit orthonormal bases for spaces of functions that are totally symmetric under the rotational symmetries of a platonic solid," *Acta Cryst.*, vol. A52, pp. 221–235, 1996.

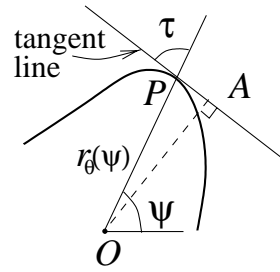


Fig. 1. Relation between tangent line and $h_{\theta}(\psi)$.

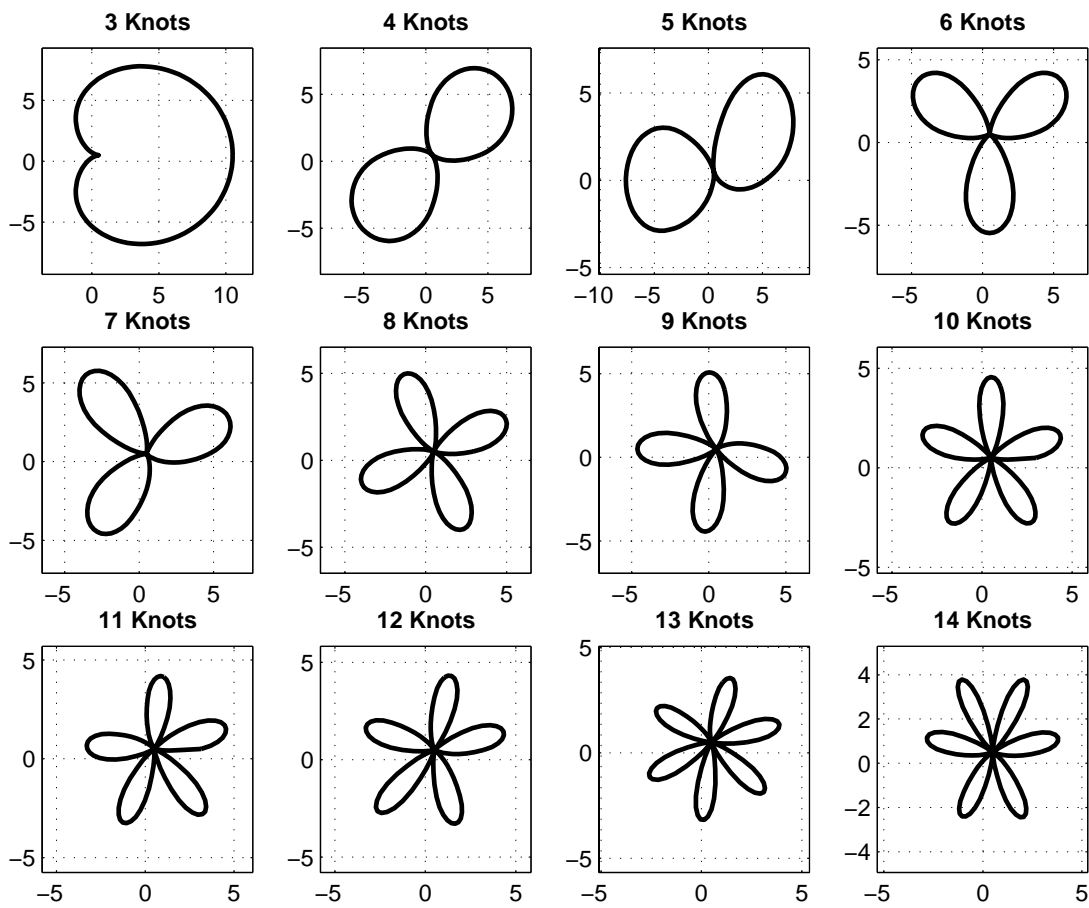


Fig. 2. Collection of worst shapes based on minimizing trace of Fisher information using iterative algorithm for the finite dimensional case. All shapes have the same perimeter. These shapes are represented by quadratic B-splines basis.

Plot of $f_B(\phi)$ for various number of knots

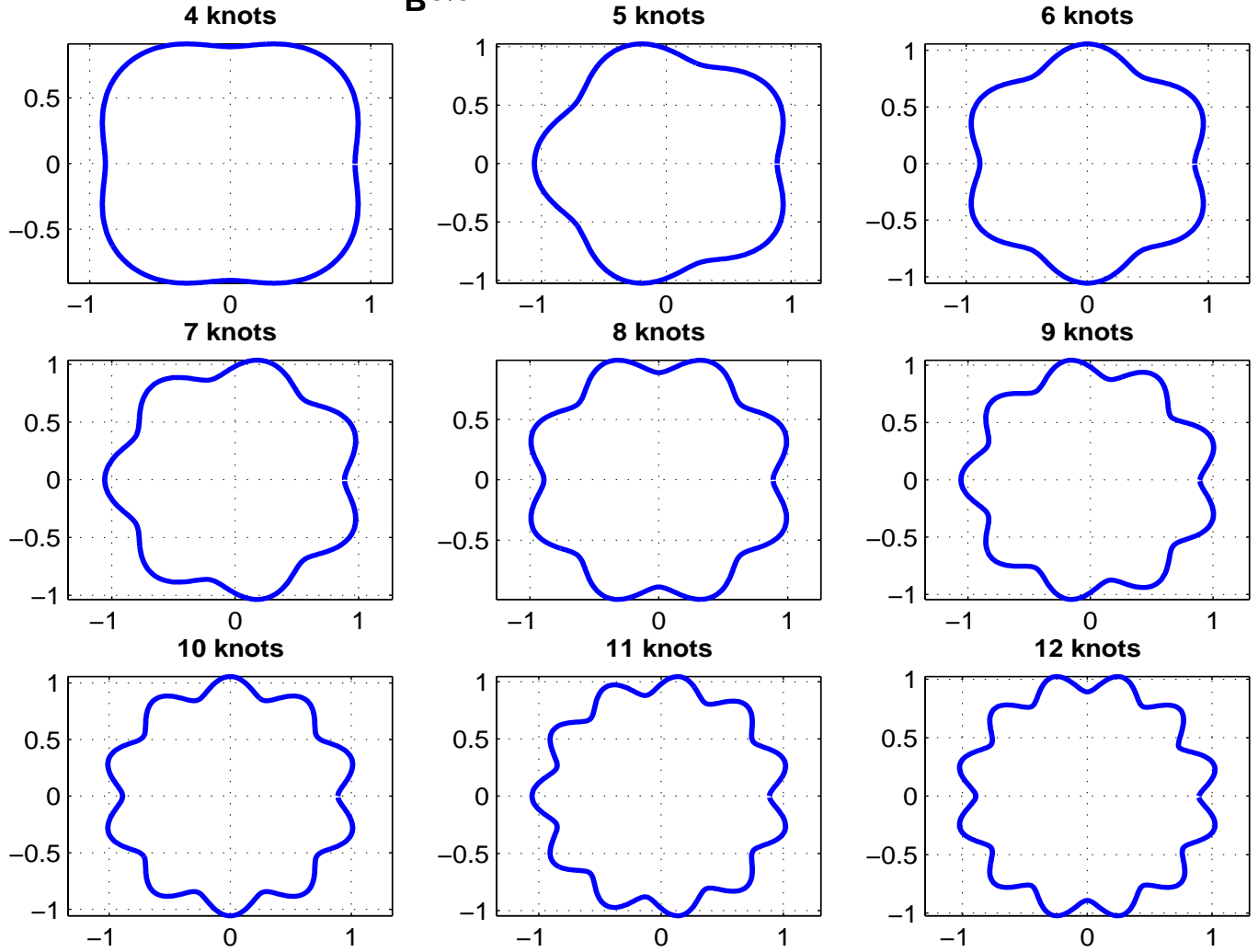


Fig. 3. Plot of $f_B(\cdot)$ for quadratic B-splines with equally spaced knots.

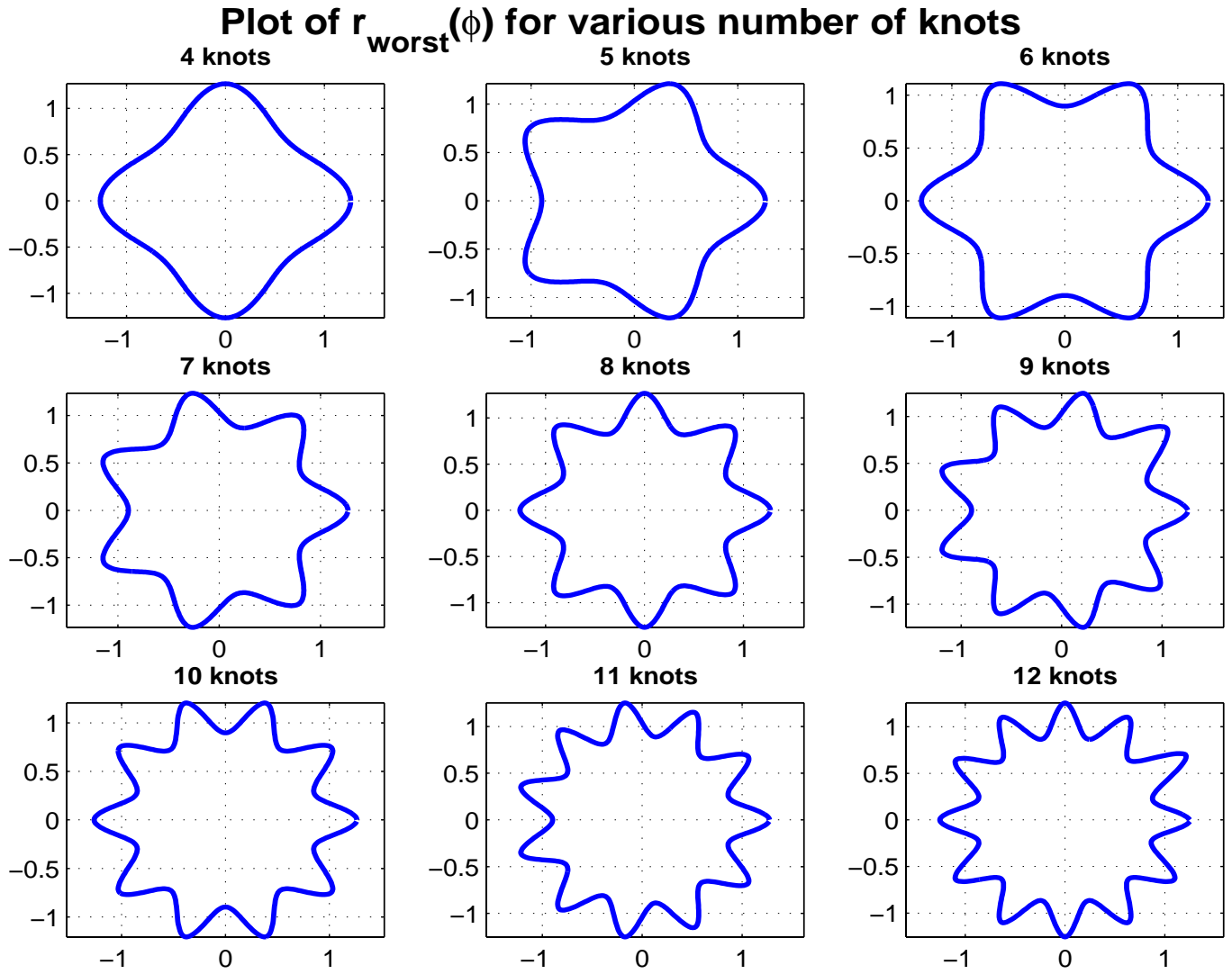


Fig. 4. Worst-shapes local to a circle for finite dimensional case with quadratic B-splines and equally spaced knots.

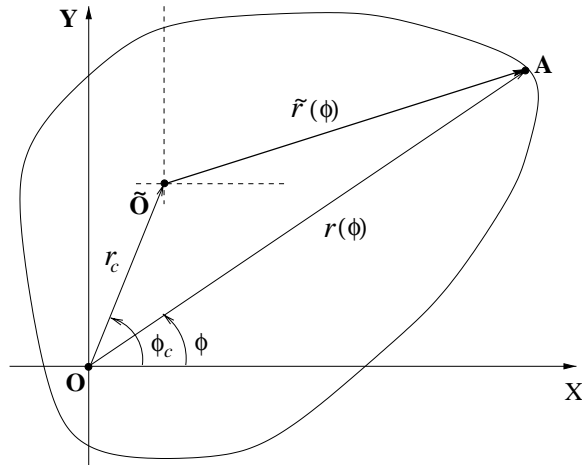


Fig. 5. Change of center-of-description.

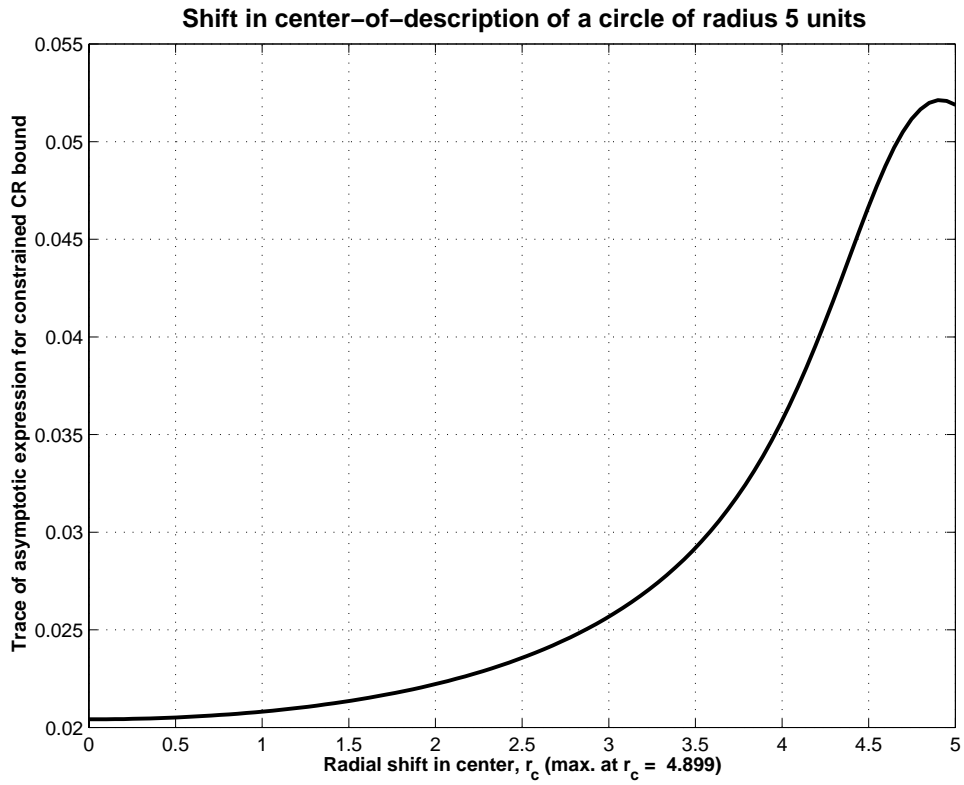


Fig. 6. Sensitivity of CR bound to shift in center-of-description of a disk-shaped object.

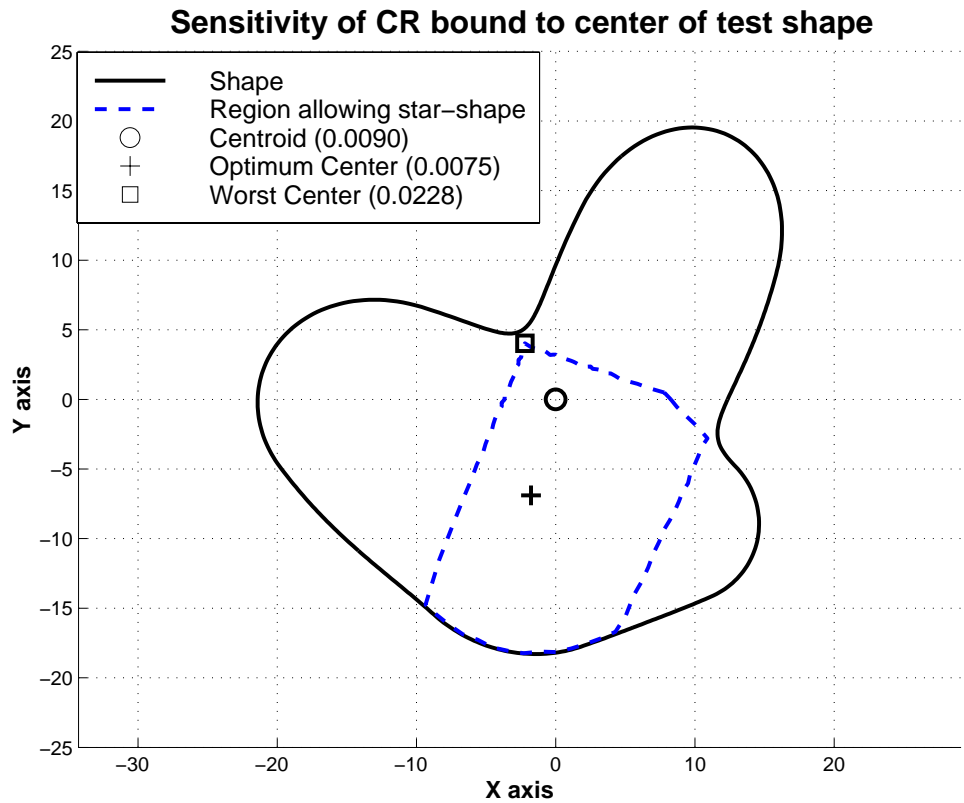


Fig. 7. Sensitivity of CR bound to shift in center-of-description of a test shape. The region delimited by a dotted line is the collection of all possible centers-of-description for which the test shape can be represented as a star-shape.

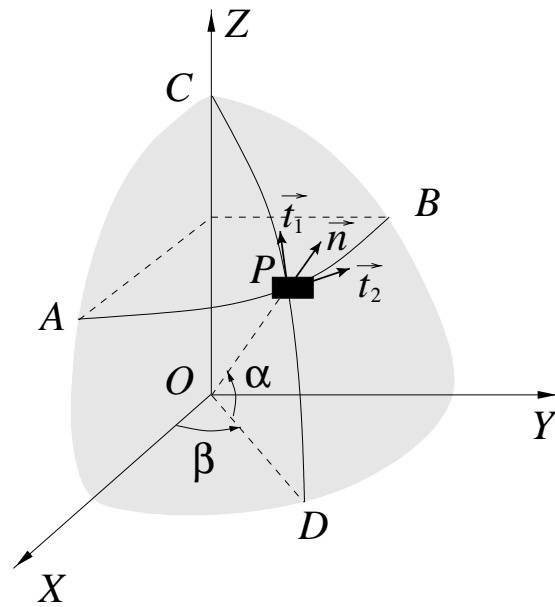
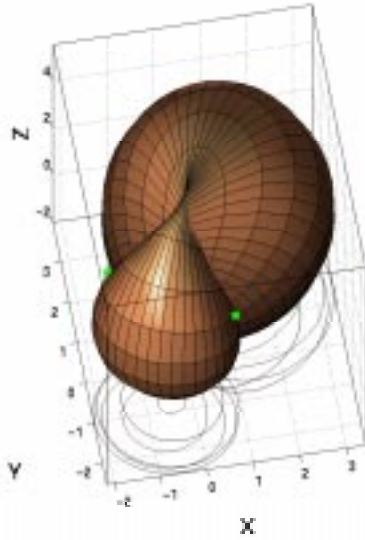


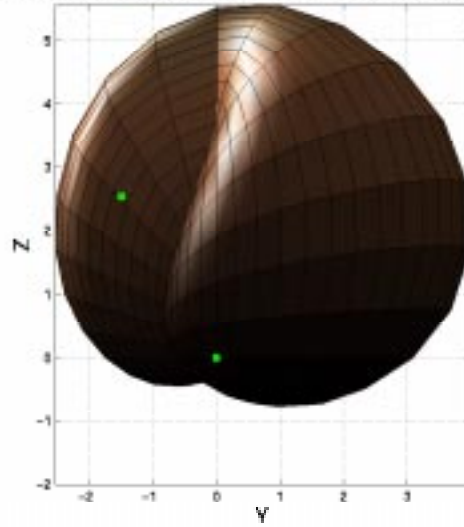
Fig. 8. Unit tangent and normal vectors for a spherical surface through P . Here, O is the center of the sphere as well as the center-of-description.

Worst shape for 3 knots (equal for azimuth and elevation basis)



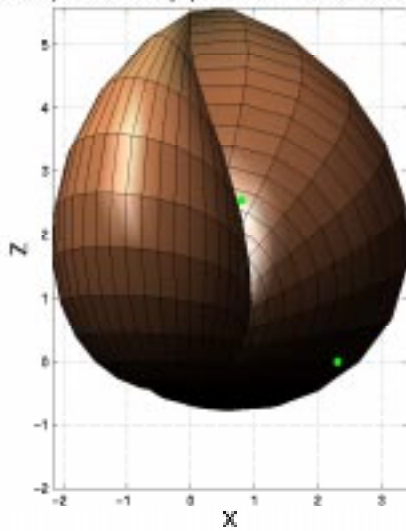
(a) View from an angle

Worst shape for 3 knots (equal for azimuth and elevation basis)



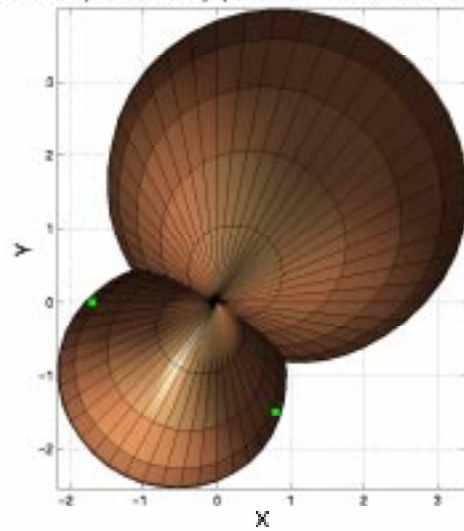
(b) View from X-axis

Worst shape for 3 knots (equal for azimuth and elevation basis)



(c) View from Y-axis

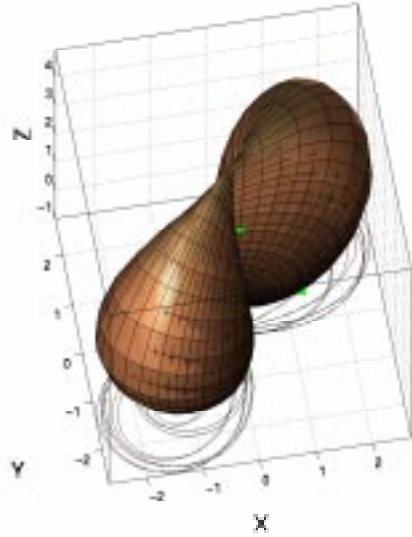
Worst shape for 3 knots (equal for azimuth and elevation basis)



(d) View from Z-axis

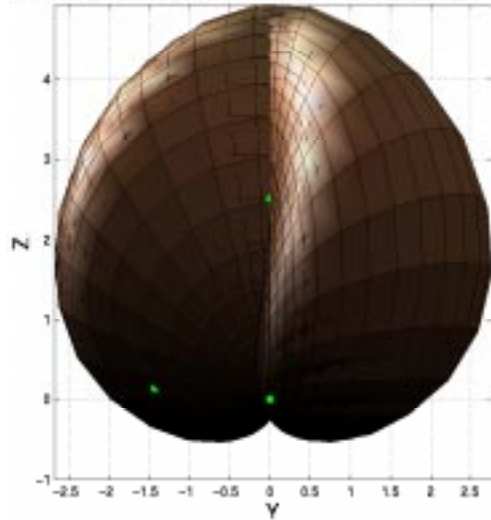
Fig. 9. Different views of worst-shape for 3×3 knots. Knot positions are marked as light colored boxes.

Worst shape for 4 knots (equal for azimuth and elevation basis)



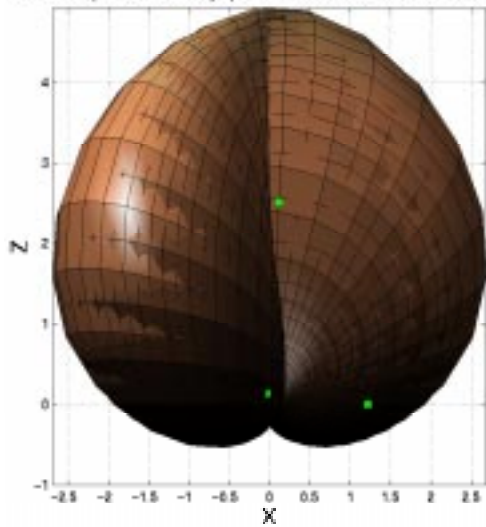
(a) View from an angle

Worst shape for 4 knots (equal for azimuth and elevation basis)



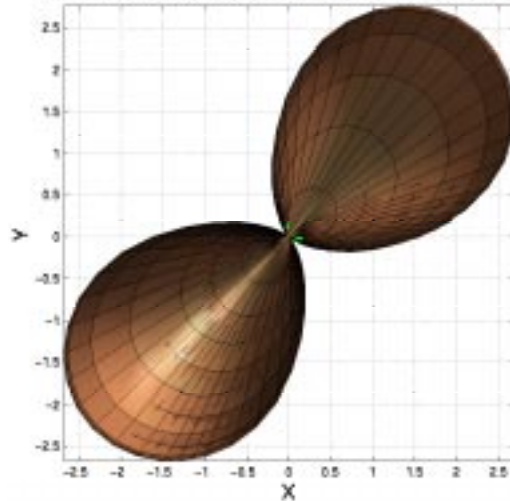
(b) View from X-axis

Worst shape for 4 knots (equal for azimuth and elevation basis)



(c) View from Y-axis

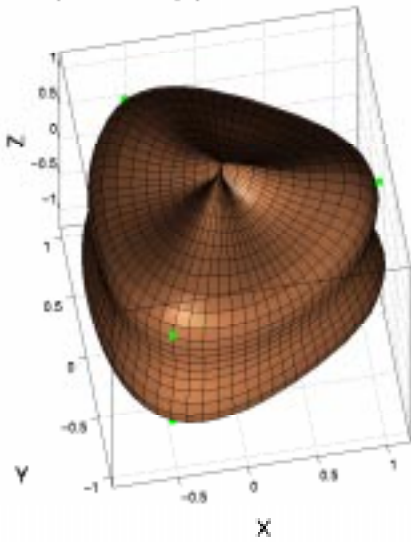
Worst shape for 4 knots (equal for azimuth and elevation basis)



(d) View from Z-axis

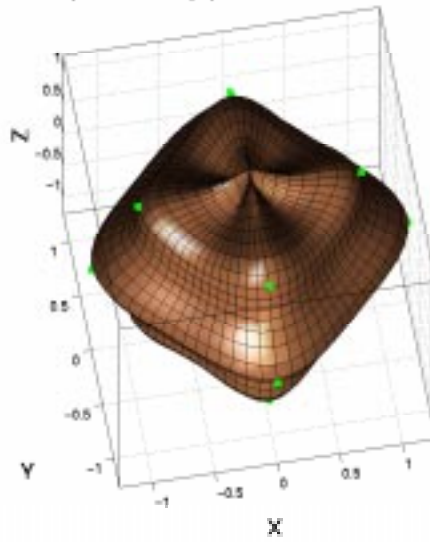
Fig. 10. Different views of worst-shape for 4×4 knots.

Worst shape for 3 knots (equal for azimuth and elevation basis)



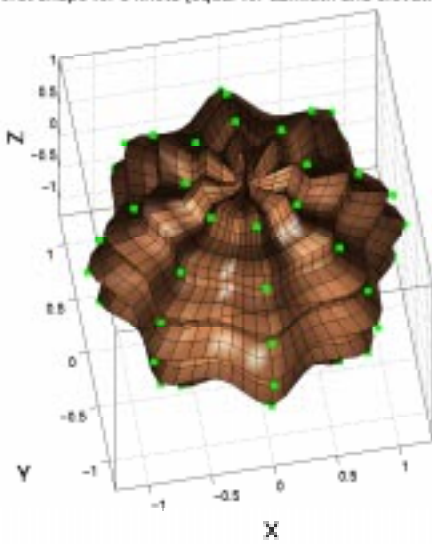
(a) 3×3 Knots

Worst shape for 4 knots (equal for azimuth and elevation basis)



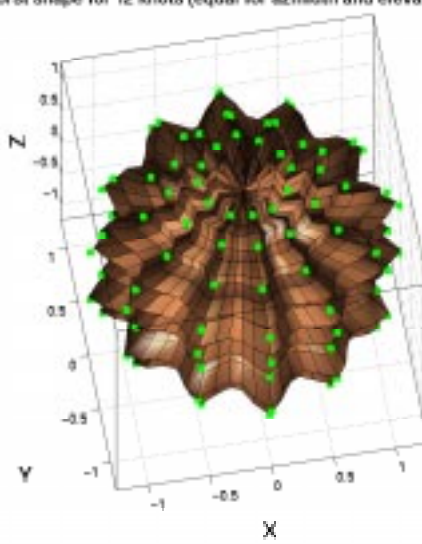
(b) 4×4 Knots

Worst shape for 8 knots (equal for azimuth and elevation basis)



(c) 8×8 Knots

Worst shape for 12 knots (equal for azimuth and elevation basis)



(d) 12×12 Knots

Fig. 11. Worst-shapes local to a sphere.